INFORMATION TO USERS

This manuscript has been reproduced from the microfilm master. UMI films the text directly from the original or copy submitted. Thus, some thesis and dissertation copies are in typewriter face, while others may be from any type of computer printer.

The quality of this reproduction is dependent upon the quality of the copy submitted. Broken or indistinct print, colored or poor quality illustrations and photographs, print bleedthrough, substandard margins, and improper alignment can adversely affect reproduction.

In the unlikely event that the author did not send UMI a complete manuscript and there are missing pages, these will be noted. Also, if unauthorized copyright material had to be removed, a note will indicate the deletion.

Oversize materials (e.g., maps, drawings, charts) are reproduced by sectioning the original, beginning at the upper left-hand corner and continuing from left to right in equal sections with small overlaps.

ProQuest Information and Learning
300 North Zeeb Road, Ann Arbor, MI 48106-1346 USA
800-521-0600

KINETICS OF THE LIQUID PHASE OXIDATION OF ETHANOL ON A PALLADIUM-ON-ALUMINA CATALYST

By

HSU, Shih-Hau

A thesis submitted to the School of Graduate Studies in partial fulfillment of the requirements for the degree of

MASTER OF APPLIED SCIENCE

in the

DEPARTMENT OF CHEMICAL ENGINEERING
UNIVERSITY OF OTTAWA

1977

ABSTRACT

The oxidation of ethyl alcohol has been studied in an aqueous phase containing sodium carbonate over the temperature range 25 to 45 °C, using a stirred semibatch reactor with four baffles containing 0.5% Pd-Al_2O_3 catalyst pellets.

The intrinsic kinetic equations were derived empirically using the rate measurements of a stirred slurry reactor in which finely crushed pellets were suspended. The oxidation rate was found to be first order with respect to dissolved oxygen concentration which varied from 3.5 to 18.5 mg/liter.

Both the gas-liquid interface and the liquid-particle surface mass transfer resistances were evaluated and found to be negligible.

The measured effectiveness factor for the pellets, which was estimated by the ratio of reaction rate of the pellet system to that of the powder system, could be brought into agreement with theory by using a tortuosity value of 2.9.

ACKNOWLEDGEMENTS

The author wishes to express his sincere appreciation to Dr. John A. Ruether for his advice, encouragement, and guidance during the course of this work. He also expresses his grateful acknowledgement to Dr. W. Hayduk for his suggestion and discussion.

Meanwhile, thanks are due to all member of the Department of Chemical Engineering for their assistance. Finally, the author is grateful to Mr. G. Gasperetti for his technical assistance in constructing the experimental apparatus used in this study.

TABLE OF CONTENTS

Page

Page

LIST OF FIGURES

LIST OF TABLES

NOMENCLATURE

NOTATION

a_1, a_2, a_3, a_4	constants in Eq. (5-5)
a_g	gas-liquid interfacial area per unit volume of liquid, cm^2/cm^3
a_p	total apparent external surface area of pellets catalyst per unit volume of liquid, cm^2/cm^3
A_p	external surface area per pellet, cm^2
B_{sec}	time needed to consume 1 cm^3 pure oxygen in bubble-meter at temperature T_B and pressure $P_{O_2,B}$, sec.
C	concentration, mol/cm^3, mg/l.
C_Z	concentration of benzoic acid in water, g/g of solution
d	diameter of particle, cm, micron
$\bar{d}$	mean diameter of particle, cm, micron
D_{Z,H_2O}	molecular diffusivity of benzoic acid in water, cm^2/sec
$D_{O_2,sol.}$	molecular diffusivity of oxygen in solution at "standard reaction conditions", cm^2/sec
$D_{O_2,eff}$	effective diffusivity of oxygen in solution, cm^2/sec. $D_{O_2,eff} = D_{O_2,sol.} \, \theta / \tau$

E	electrode potential vs. saturated calomel electrode, volt
$\Delta G^0_{25\ ^oC}$	standard free energy of a reaction at 25 ^oC, KCal./g-mol
H	Henry's law constant, atm./(g-mol/l.)
J	number of active sites
K	kinetic constant (See Eq. (5-5))
K_1, K_2	equilibrium constants for adsorption in Eq. (5-5)
K_L	gas-liquid mass transfer coefficient, cm/sec
K_p	fluid-particle mass transfer coefficient, cm/sec
K_v	kinetic rate constant
$K_{v,app}$	apparent kinetic rate constant measured with internal diffusion
L	effective thickness of the shell, ratio of catalyst volume to outside surface through which reactant has access, cm
m	power law reaction order
n	mole
N_p	number of particles
$\bar{p}$	saturated water vapor pressure, mm Hg
P	barometric pressure, mm Hg
$P_{O_2,B}$	partial pressure of oxygen in bubble-meter B, mm Hg

$P_{O_2,r}$	partial pressure of oxygen in the reactor, atm
q	ratio, $= C_{b,Z} / C_{s,Z}$
r	reaction rate of oxidation, mol/(sec)(cm^3-cat)
r_p	rate of mass transfer of benzoic acid to water, mg/(sec)(cm^3)
r_v	rate of reaction per unit volume of liquid, mol/(sec)(cm^3)
R	universal gas constant, (cm^3·atm)/(^oK·mol)
S, S'	solubility of oxygen, mg/l.
S_m	internal surface area of the catalyst per unit volume of liquid, cm^2/cm^3
Sh	Sherwood number, $= d\ K_p / D_{AB}$
t	time, sec
T	absolute temperature, K
T_B	temperature of oxygen in bubble-meter B, ^oC
T	transport factor, $= C_s/C_b$
V	volume, cm^3
V^o	initial volume of oxygen read on the bubble-meter, cm^3
V_L	volume of liquid solution, cm^3
X	distance from catalyst surface, cm
W	weight of catalyst, g

GREEK LETTERS

η	internal effectiveness factor
θ	internal void fraction of catalyst, porosity factor
μ	viscosity, c.p.
ξ	intrinsic reaction rate per unit internal area of catalyst, mol/(sec)(cm^2)
ρ_p	bulk density of pellet catalyst, g/cm^3
τ	tortuosity factor
ϕ	Thiele diffusion modulus, ϕ_s for sphere $= \frac{d}{2}\sqrt{\frac{K_v C_s^{m-1}}{D_{eff}}}$ ϕ_L for flat plate geometry $= L\sqrt{\frac{K_v C_s^{m-1}}{D_{eff}}}$
Φ_s	Weisz modulus for spherical particle, $= \frac{d^2}{4 D_{eff}} \left(\frac{-1}{V_c} \frac{d n}{d t}\right) \frac{1}{C_s}$

SUBSCRIPTS

avg	average
b	bulk liquid
B	bubble-meter B
c	catalyst
Et	ethanol

max	maximum
N	sodium carbonate
O_2	oxygen
p	particle
pellet	pellet system
powder	powder system
r	reactor
s	particle external surface; sphere
sol.	"standard reaction conditions" consisting of 0.6 molar ethanol and 0.1 molar Na_2CO_3
Z	benzoic acid
*	equilibrium value for concentration

I. INTRODUCTION

Solid oxidation catalysts have recently been developed for oxidizing small concentrations of organic pollutants in liquid water. This provides an opportunity for developing an alternate process to bacterial oxidation. Of particular importance in developing the process is the optimum type reactor to use; fixed-bed, slurry, or trickle-bed. Mass transfer resistances differ in each type of reactor. Their significance with respect to the chemical kinetics at the catalyst site needs to be determined before optimum reactor types can be determined. Research in this area would involve studying the kinetics for pollutant removal with the solid catalysts, measuring mass transport rates, and reactor modeling to give optimum design results. Removal of small quantities of organic compounds dissolved in water (such as acids, aldehydes, hydrocarbons) has become an important industrial problem due to more strict regulations concerning discharge of industrial wastewaters into streams, bays, etc..

Consequently, slurry reactors are becoming of importance for various types of catalytic reactions, including pollutant oxidation. While such reactors have advantages of capacity and isothermal operation, transport resistances can severely affect the rate of reaction, and hence, the design of equipment. A number of research problems are available which have the objective of evaluating mass transfer resistances in slurry reactors. Such resistances include mass transfer

between bulk fluid and outer surface of catalyst particle, intraparticle mass transfer in liquid-filled pores, and gas bubble to bulk liquid transport. Transient methods appear to be well-suited for studying mass transport in slurry reactors. The new technique of pulse testing can lead to considerably more information than is obtained by conventional, steady-state measurements. Theoretical as well as experimental work is needed to develop these methods.

Hydrotreating of hydrocarbons, on the other hand, is often performed industrially in trickle bed reactors, especially for heavy, high boiling hydrocarbon fractions. To keep internal effectiveness factors for the catalyst as high as possible, the catalyst particles are kept as small as possible, a lower limit on catalyst size being imposed by the fact that pressure drop through the bed increases as particle size decreases. Sometimes extrudates with diameter as small as 1/16-inch are used. Even with the use of small catalyst particles, effectiveness factors much less than unity often obtain. There have not been many complete studies of internal diffusion resistance in hydrotreating heavy fractions. It is possible that either hydrogen or the hydrocarbon reactant could be the diffusion limiting reactant, in general. Hydrogen concentration is low compared to that of the hydrocarbon reactant. A compensating factor, however, is that the diffusivity of hydrogen is much greater than the hydrocarbon.

Another approach to achieving high internal effectiveness factors in a fixed-bed, gas-liquid reactor is to use catalyst particles that contain active catalytic components in a thin shell only, i.e. of the order of 100 microns in thickness, the shell being deposited about the external, geometric surface of the catalyst support particles. By this approach, relatively large particles could be used, so pressure drop in the reactor would not be excessive. However, internal effectiveness factors could be made to approach unity as closely as desired by making the catalytically active layer sufficienty thin.

In the project described as follows, using a stirred semibatch reactor, kinetic data and data on internal effectiveness factors will be gathered for the oxidation of ethanol on a palladium-on-alumina catalyst deposited as a layer on an inert support particle. This reaction has been chosen because it proceeds smoothly at room temperature and relatively low pressures, and hence is safer and more convenient for basic research than a hydrogenation reaction. Furthermore it was hoped that the results of this work might be used in a later project, where the same reaction will be carried out in a trickle-bed reactor, under conditions of pulsing flow.

2. PREVIOUS WORK WITH THE OXIDATION OF ETHANOL ON PRECIOUS METAL CATALYSTS

A good introduction to reactor design in gas-liquid-solid catalytic systems has been given by Østergaard[1]. In this study, a model reaction was carried out in a semibatch stirred reactor. Mass transfer resistances were measured, and experimental conditions were chosen such that intrinsic kinetics could be determined without mass transfer limitations. The reaction used was the oxidation by gaseous oxygen of aqueous solutions of ethanol with a supported palladium catalyst. A review of previous work on this reaction follows.

2.1 Model Reaction

A liquid-phase oxidation was chosen as model reaction, according to the investigation of Klassen and Kirk[2]. Ethanol in an aqueous sodium carbonate solution was oxidized to acetic acid by palladium-on-alumina catalyst, which then reacted with the sodium carbonate to produce sodium acetate homogeneously.

$$C_2H_5OH + O_2 + Na_2CO_3 \xrightarrow{Pd\text{-}Al_2O_3} CH_3COONa + NaHCO_3 + H_2O \qquad (2\text{-}1)$$

The thermodynamic data[3] at 25 °C for the reaction

$$C_2H_5OH_{(aq.)} + O_{2(g)} + Na_2CO_{3(aq.)} \xrightarrow{Pd\text{-}Al_2O_3}$$

$$CH_3COONa_{(aq.)} + NaHCO_{3(aq.)} + H_2O_{(l)} \quad (2\text{-}2)$$

shows that $\Delta G^{o}_{25\ ^{o}C} = -118.7$ Kcal./g-mol. The thermodynamic equilibrium constant has a value of 1×10^{87}; consequently the reverse reaction may be neglected.

The choice of palladium as the catalyst was based on work of Mueller and Schwabe[4], who oxidized ethanol in a batch reactor using various platinum-group metals as catalysts. Their work indicated that any of these metals could be used as catalysts, but all catalysts with the exception of palladium required an incubation period. Klassen and Kirk found that alumina would not interfere by catalyzing the reaction, and they used a palladium-on alumina catalyst containing 5% palladium. In their work, the alumina carrier was in the form of irregularly shaped particles, 1/8 to 1/4 in. in size.

Mueller and Schwabe also tried acid, alkaline and neutral reaction media. They found that in a neutral solution no reaction occurred; in acid solution, the ethanol was oxidized to acetaldehyde; and in basic solution, acetic acid was formed. It was desirable to produce acetic acid as the product of the reaction because of the simplicity of analysis. Thus it appeared necessary to used a basic solution for the experiments.

Klassen and Kirk found that even dilute sodium hydroxide solutions attacked the alumina carrier. Ammonia inhibited the reaction completely. Various lower amines were tried, and while these did not inhibit the reaction they proved so volatile that extra precautions had to be taken to prevent substantial loss and consequent errors in analysis. Sodium carbonate was then tried and proved to be successful. Concentrations usually of the order of 0.1 molar were used. No attack on the carrier was noticed and the ethanol oxidized was completely converted to the acetic acid. Aldehyde and ketone tests gave negative results; analytical tests by the Chemistry Department at the University of Wisconsin confirmed the presence of acetate ions.

Recently, this model reaction had been studied by Sato et al.[5] under the condition of a fixed-bed catalytic reactor with cocurrent gas-liquid flow. They used spherical particles of catalyst containing 5% palladium supported on alumina (diameter 3.8 mm). It was also found that the liquid-phase oxidation of ethanol on palladium catalyst proceeds in first-order regime with respect to oxygen under certain conditions.

2.2 Introduction To Slurry Reactor

The slurry reactor may assume various forms (stirred tank, bubble column, sieve-tray staged reactor), but

whatever the reactor geometry, the reaction phases are gas, solid, and liquid, i.e., solid catalyst is suspended in a liquid medium within which gas is dispersed. Slurry reactors offer several advantages not enjoyed in alternative modes of operation:[8]

(1) A high heat capacity to provide good temperature control

(2) A potentially high rate of reaction per unit volume of reactor if the catalyst is highly active

(3) Easy heat recovery

(4) Adaptability to either batch or flow processing

(5) The catalyst may be readily removed and replaced if its working life is relatively short, and

(6) They may permit operation at catalyst effectiveness factors approaching unity, of especial importance if diffusion limitations cause rapid catalyst degradation or poorer selectivity.

Their disadvantages are that:

(1) The residence time distribution patterns are close to those of a continuous stirred-tank reactor which makes it difficult to obtain high degree of conversion except by staging.

(2) Catalyst removal by filtration may pose problems with possible plugging difficulties on filters, and the costs of filtering systems may be a substantial

portion of the capital investment, and

(3) The high ratio of liquid to solid in a slurry reactor allows homogeneous side-reactions to become more important if any are possible.

Compared to the description of a two-phase reaction system with a microporous catalyst, the description of a three-phase reaction system has the added consideration of mass transfer between the gas and liquid phases. The rate of transfer of a reactant from the gas phase to the bulk liquid phase is governed by the product of gas absorption coefficient and gas-liquid interfacial area, $K_L a_g$. To reach the exterior surface of a catalyst particle, reactants dissolved in the liquid phase must overcome fluid particle mass transfer resistance arising from the liquid boundary layer surrounding the particles. Finally, within a porous catalyst particle there is a kinetic resistance, and an intraparticle diffusion resistance.

Since the two external diffusion steps act in series with the diffusion and reaction step within the catalyst, the rates of the three steps must be equal under steady conditions. For the reaction, $A + O_2 \longrightarrow P$, the rate per unit volume of liquid can be written

$$r_v = K_L a_g (C_{O_2,*} - C_{O_2,b}) \qquad (2\text{-}3)$$

$$= K_p a_p (C_{O_2,b} - C_{O_2,s}) \qquad (2\text{-}4)$$

$$= S_m \eta \xi (C_{O_2,s} , C_{A,s}) \qquad (2\text{-}5)$$

where $\xi(C_{O_2,s} , C_{A,s})$ is the intrinsic reaction rate when both reactants are at the concentrations existing at the outer surface of the catalyst particle.

In summary, both mass transfer and kinetic resistances are important in the design of this type of reactor. Furthermore, the effects of external and internal particle mass transfer resistance on rate for hydrogenations carried out on finely divided catalysts in slurry reactors were treated by Ruether and Puri[6].

3. EXPERIMENTAL APPARATUS AND MATERIALS

3.1. The Reactor

An agitated vessel of one gallon capacity, as shown in Fig.3-1, was a cylindrical stainless steel tank of height 24.4 cm and diameter 16 cm. The vessel was filled to a depth of 16 cm in order to keep the ratio of vessel diameter to solution depth at unity.

Two flat-bladed impellers with six blades, diameter 7 cm, one placed one-third of the distance from the bottom to the liquid level, and the another placed at the level of gas-liquid interface to increase the contact interface, were driven by a variable speed motor.

Four symmetrically placed verticle baffles of width 1.6 cm and length 21.0 cm, made of stainless steel seive were used. The baffles were in the form of hollow cylinders into which catalyst particles or glass spheres could be placed.

A gas sparger was located under the bottom impeller near its tip. Also another gas injection point to the reactor consisted of a nozzle 1.5 cm above the liquid reactant surface.

3.2 Temperature Control System

The reactor had an insulated water jacket for heating

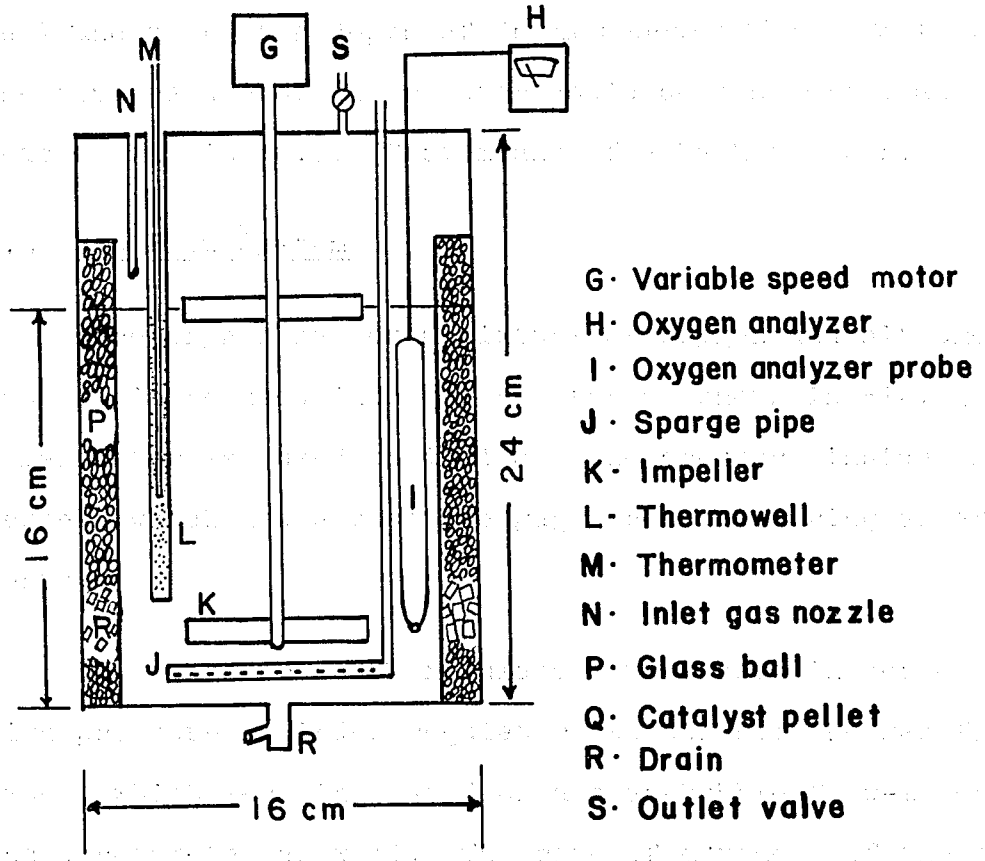

Fig. 3-1 THE REACTOR.

or cooling. It was used with a thermal bath of controlled temperature (accurate to 0.01 ^{o}C). A high-precision thermometer was carefully inserted in the thermo-well and kept at a depth of 76 mm beneath the liquid level. The temperature of the reactor could be controlled and read to within ±0.01 ^{o}C by means of a kathetometer.

3.3 Gas Flow System

Pure oxygen gas or a mixture of oxygen and nitrogen gas was introduced into the reactor as shown in Fig. 3-2. A manometer was used to indicate the pressure inside the vessel, which had a positive gage pressure during experiments.

Low range pressure regulators were used in series with high pressure cylinder regulators to control the gas flow rates, which were indicated on a soap-bubble flow-meter, and a rotameter as well. The rate of movement of the film inside the soap-bubble flow-meter tube, which could be determined by means of a stopwatch and a kathetometer, was exactly equal to the rate of flow of gas. It should be noted that the room temperature changed within ±0.03 ^{o}C during each run, therefore the measurements of oxygen absorption consumption could be treated as carried out in a constant temperature room.

a) Low pressure regulator
b) Rotameter
c) Manometer
d) Rubber bulb
e) Bubble-meter
f) Stainless steel mesh
g) Motor
h) Oxygen analyzer
r) Drain

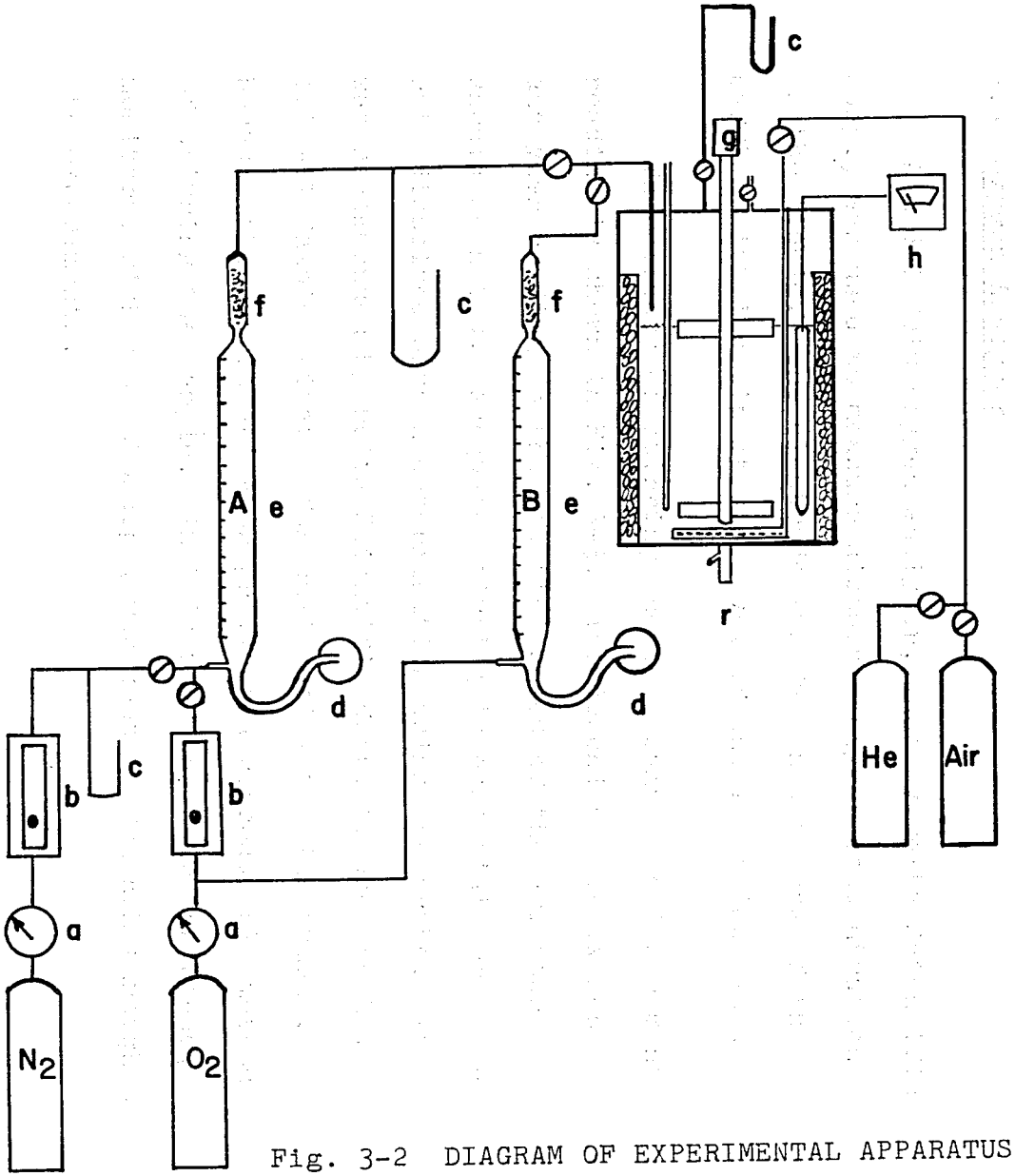

Fig. 3-2 DIAGRAM OF EXPERIMENTAL APPARATUS.

3.4 Oxygen Analyzer

A model 2010 oxygen analyzer, made by Delta Scientific Corp., was used to measure dissolved oxygen concentration in the liquid. The electrode was fastened to one of the baffles with its tip at the level of the lower impeller.

The effects of stirring the test sample on instrument reading is shown in Fig. 3-3. The dependence of oxygen analyzer reading on the rotating speed of the agitator should be noted. Adequate stirring is essential for accurate dissolved oxygen determination using the probe. It was recommended by Delta Scientific Corp. to use the No. 1010-11 Sample Agitator for calibrating the instrument, because the sample agitator provides a reproducible method of stirring the sample. In this work the stirring speed, monitored with a stroboscope, was kept at 203 RPM throughout the experiments.

Calibration values[7] for dissolved oxygen concentration in distilled water over the temperature range from 21 ^{o}C to 50 ^{o}C are shown in Table 3-1. For results of highest accuracy, correct the results in accordance with the formula which involves atmospheric pressure shown at the bottom of Table 3-1.

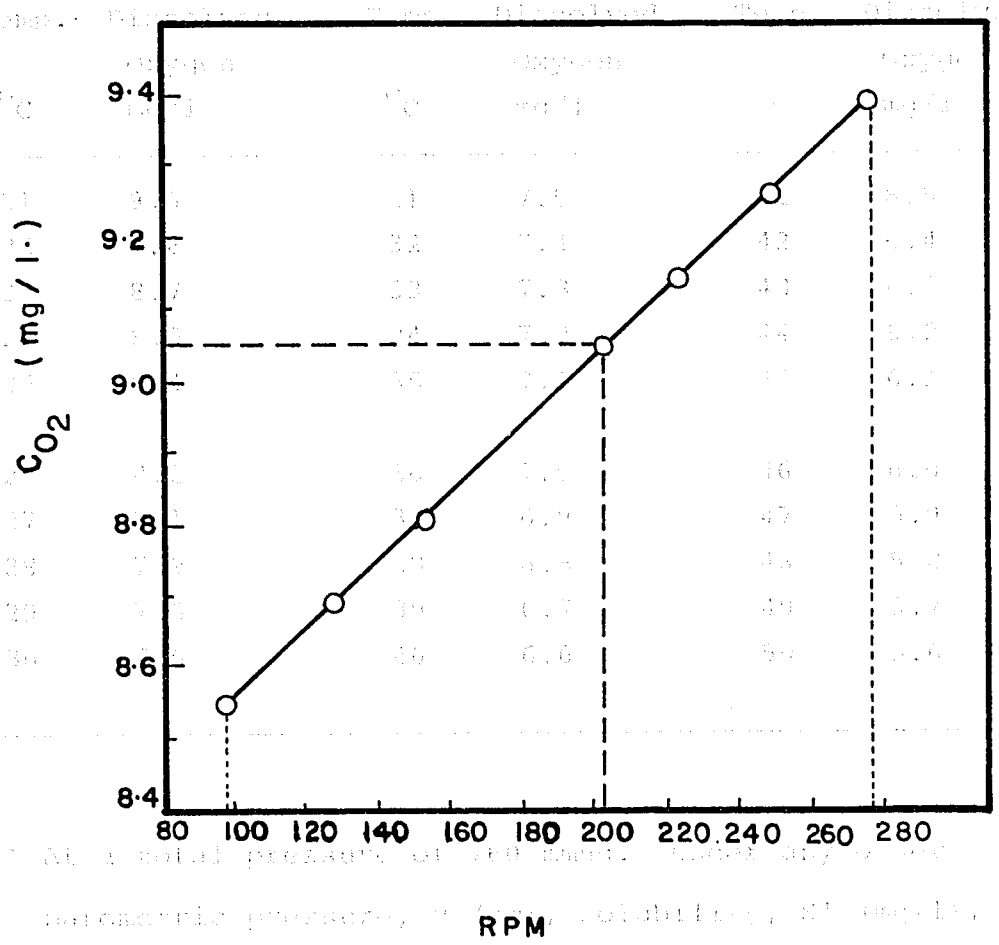

Fig. 3-3 Rotating speed of impeller vs. indicated dissolved oxygen concentration at 21 °C and barometric pressure at 764.12 mm Hg.

TABLE 3-1 Solubility of Oxygen in Distillated Water Exposed to Water-Saturated Air[§]

Temp. °C	Dissolved Oxygen mg/l	Temp. °C	Dissolved Oxygen mg/l	Temp. °C	Dissolved Oxygen mg/l
21	9.0	31	7.5	41	6.5
22	8.8	32	7.4	42	6.4
23	8.7	33	7.3	43	6.3
24	8.5	34	7.2	44	6.2
25	8.4	35	7.1	45	6.1
26	8.2	36	7.0	46	6.0
27	8.1	37	6.9	47	5.9
28	7.9	38	6.8	48	5.8
29	7.8	39	6.7	49	5.7
30	7.6	40	6.6	50	5.6

[§] At a total pressure of 760 mmHg. Under any other barometric pressure, P (mm), solubility, S' (mg/l), can be obtained from the corresponding value in the table by the equation:

$$S' = S\frac{P - \bar{p}}{760 - \bar{p}}$$

in which S is the solubility at 760 mm Hg. and the $\bar{p}$ is the pressure (mm) of saturated water vapor at the temperature of the water. Dry air is assumed to contain 20.90 per cent oxygen.

3.5 Catalyst

The catalyst used (0.5 %wt Pd on Al_2O_3) was in the the form of cylindrical pellets (1/8 by 1/8 in. or 0.32 by 0.32 cm nominal dimensions) manufactured by U.S. Engelhard Company. By microscopic observation of a number of cleft pellets, the penetration of palladium was found to be confined to a relatively thin shell, some 0.0367 cm depth on the outer surface of the pellet, as shown in Fig. 3-4. However, an effective thickness of the shell, L, was defined as the ratio of metal catalyst volume to outside surface area through which reactant has access.[24] The volume of this catalyst layer corresponded to 51.3% of the total pellet volume. The physical properties of the catalyst are summarized in Table 3-2.

For the intrinsic kinetic studies, the pellets were ground in an electric-mortar into small particles, which were collected after passing through a sieve of 88 micron mesh opening. The finely crushed pellets were suspended in a slurry reactor.

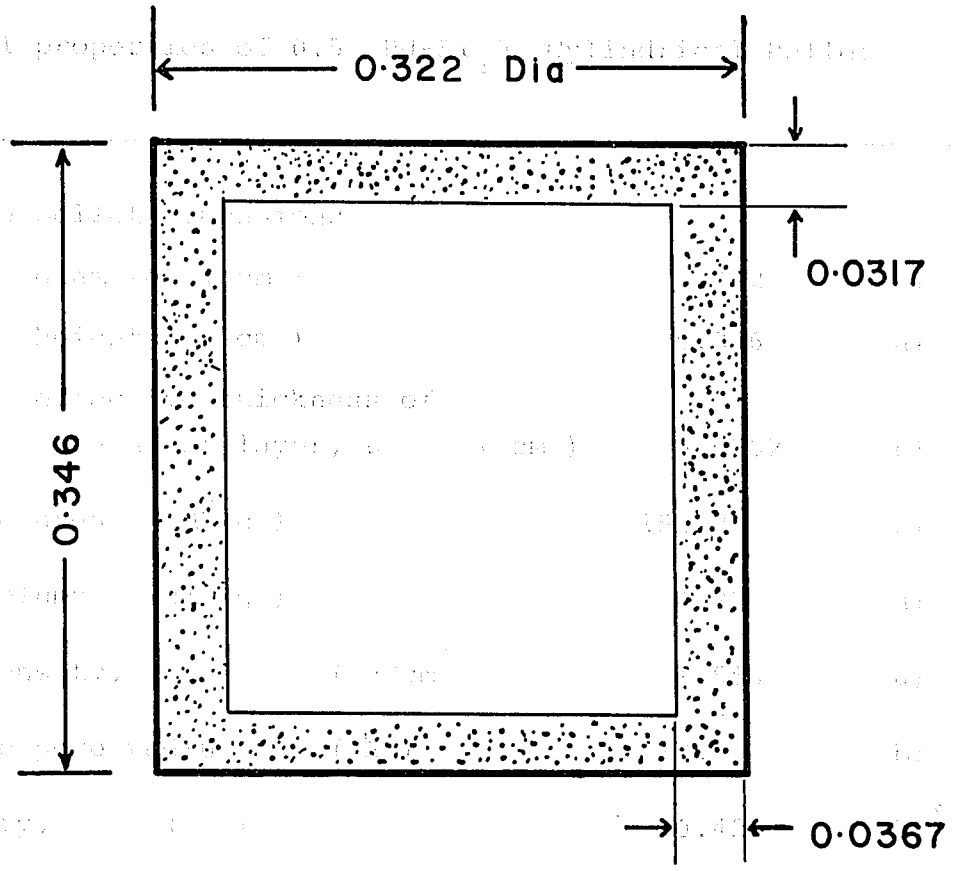

Dimension: cm

Fig. 3-4 AVERAGE PELLET DIMENSIONS.

TABLE 3-2

Physical properties of 0.5% Pd-Al_2O_3 Cylindrical Pellet

Average pellet dimensions		
diameter (cm)	0.322	a)
height (cm)	0.346	a)
effective thickness of Catalyst layer, L (cm)	0.0282	b)
Surface area (M^2/g)	152.2	a)
Pore volume (cm^3/g)	0.272	a)
Bulk density, (g/cm^3)	1.556	a)
Average pore radius (Å)	18.0	b)
Porosity, (-)	0.423	b) §

a) measured value

b) calculated value

§ Detail given in Appendix I-D

4. PROCEDURE AND PRELIMINARY EXPERIMENTS

4.1 Mass Transfer Effects

4.1.1 Determination of the gas-liquid mass transfer resistance

The gas-liquid mass transfer resistance may be determined by observation of the rate of absorption of a soluble gas into the solute-free liquid, and physical absorption is a method which has been used extensively in the determination of the mass transfer coefficient.

Before a run, the baffles in the reactor contained glass balls without catalyst. The gas nozzle was not placed in the reactor during the study of gas absorption rates. The liquid was distilled water containing 0.1 M Na_2CO_3.

Helium was introduced into the liquid through the sparger until the reading of the oxygen analyzer reached the minimum, i.e. 0.004 mg/l. Therefore, the liquid system could be treated as an oxygen-free solution. After enough ethanol was added to make the liquid phase concentration 0.6 M, the system was closed immediately by stopping the inlet helium, and closing the outlet valve on the reactor cover. The agitator was stopped. After a short period, the outlet valve was opened again and oxygen gas was intro-

duced for 15 sec. Next, the outlet valve was closed again, and the agitator was restarted. The volume of oxygen absorbed was recorded as a function of time until no further absorption could be detected in the bubble-meter B. The rate of absorption of oxygen, therefore, could be measured during the initial period by means of a timer, i.e. HP-55 calculator. Initial absorption rate data were plotted in a manner as given in Appendix I-A for the determination of the gas-liquid mass transfer coefficients.

4.1.2 Determination of the liquid-pellet mass transfer resistance

Particle mass transfer coefficients for benzoic acid pellets in water were measured by use of a fluorescent dye. The dye, rhodamine B, was dissolved as a 1.0 wt% solution in molten benzoic acid used to make a cast layer on the pellets. The rate of dissolution of the layer was determined using a fluorometer. Since the solubility of dye is much greater than that of benzoic acid, the rate of release of dye into solution was controlled by the rate of dissolution of benzoic acid. It was also necessary to use the pellet surface area comprising benzoic acid in calculating values of K_p from experimental data. The surface area of rhodamine B and benzoic acid were assumed to be equal to the ratio of their solid volume fractions[9]; thus the area for benzoic acid was 99% of the geometric area.

Use of a fluorescent dye has two advantages compared to the conventional method of titrating effluent liquor containing benzoic acid. Since dye can be measured quantitatively at concentrations as low as 10^{-8} g/l., this method of analysis is more sensitive than titration. For 1.0 wt % dye in benzoic acid, the lower limit of dye concentration for analysis represents a benzoic acid concentration of about 10^{-4} M. Thus with the dye technique it is possible to operate with fewer active pellets than would be required for analysis by titration.

Two active pellets having a cast layer about 0.3 mm deep were used in a test to determine the value of K_p. The average reduction in the mass of the cast layer during a run was less than 1.0% due to the short period of testing, i.e., within 2 min. Therefore, in calculations of surface area an arithmetic average of the initial and final diameters was used.

The pellets were placed in one of the baffles which were filled with glass balls. When the baffles were mounted in the reactor, the agitator was started. Samples were taken by means of sampling syringes, and were analyzed by the fluorometer. A complete description of apparatus and procedure was given by Lemay[10]. A sample calculation of particle-liquid mass transfer coefficients is given in Appendix I-B.

4.2 Kinetic Studies

4.2.1 Determination of reaction rates (slurry system)

Runs were made in the range of the operating variables shown in Table 4-1. A mixture gas of oxygen and nitrogen was introduced via the bubble-meter A into the reactor containing distilled water until the oxygen analyzer reached its first steady state reading, Then, the sodium carbonate and catalyst were fed into the reactor to reach the second steady state reading.

After solute ethanol was fed into the reactor, the system was closed immediately by means of stopping the agitator, stopping the gas feed, and closing the outlet valve on the reactor cover, Thereupon, oxidation was started by introducing pure oxygen gas through the bubble-meter B, i.e. on the right hand side of Fig. 3-2, into the reactor, and starting the agitator.

Approximately eighty minutes were allowed for the system to reach steady state, and then the data for the run were taken, The readings of bubble-meter and oxygen analyzer were recorded, as were the room temperature and the barometric pressure.

4.2.2 Determination of reaction rates (pellet system)

Generally speaking, the procedure of operating a reactor in the pellet system was the same as the last section (Sec. 4.2.1)

TABLE 4-1

Range of Experimental Variables

Reactor Temperature (^{o}C)		25.0 - 45.0
Reactor Total Pressure (mm Hg. gauge)		33.0 - 37.0
Oxygen Partial Pressure (atm.)		0.08 - 0.6
Dissolved Oxygen Concentration (mg/l.)		3.5 - 18.5
Solution Volume (cm^3)		2700.0
Ethanol Concentration in Solution (mol/l.)		0.45 - 1.80
Na_2CO_3 Concentration in Solution (mol/l.)		0.01 - 0.40
Catalyst Loading (g)	For Powder Runs	3.5 - 10.0
	For Pellet Runs	35.0075
Stirring Speed (r.p.m.)		203

except the catalyst pellets, i.e. 35.0075 g, were already equally placed in the four baffles near the tip of the bottom impeller.

4.2.3 Specific procedures

(1) Testing for leakage

The system was checked for possible leakage as follows

(i) After maintaining a pressure of 40 mm Hg. gage in the system, the air supply was closed. There was no indication of a pressure drop after forty hours.

(ii) Under the above conditions, there was no indication of air flowing through the bubble-meter.

(2) Reaction without palladium

In order to test the performance of catalyst, i.e. 0.5% Pd-Al_2O_3 in this study, pure alumina powder was tried in the slurry reactor system. It was found that no reaction occurred under this condition.

(3) Aldehydes and ketones test

A test was made to determine if the oxidation of ethanol yielded acetate ion exclusively. In order to get the highest yield of by-path products (if any), i.e.

aldehydes and ketones, some special runs were carried out up to thirty hours. Samples were taken during and after the run and tested by 2,4-dinitrophenylhydrazine reagent. The utility of 2,4-dinitrophenylhydrazine lies in the fact that almost all aldehydes and ketones readily yield insoluble, solid 2,4-dinitrophenylhydrazones[11]. Aldehyde and ketone tests gave negative results. Thus it could be safely assumed that all the ethanol converted was oxidized to acetic acid.

(4) Chemical analysis of feed and product

The analytical procedure was based on the conversion of ethanol to acetic acid. The conversions for some given runs were determined from the difference of carbonate ions content of the feed and product. The analysis for carbonate ions involved the potentiometric titration of the alkaline sodium carbonate solutions with acetic acid by using a glass-electrode and saturated calomel electrode pH meter as well as the thymol blue-cresol red mixed indicator[12].

An obvious method of finding the equivalence point is to plot e.m.f. (E) values as ordinate versus volume (V) of the titrant solution as abscissa , and employ the so-called "analytical" method[13] of locating the end point. The latter depends upon the fact that the second derivative, $\Delta^2E/\Delta V^2$, of the curve is zero at the end

point where the slope of the curve, $\Delta E/\Delta V$, is a maximum. Figures and detailed sample calculations of this potentiometric titration method are given in Appendix I-F. A comparison of the calculation of conversion by means of titration of unreacted carbonate ions and from volumetric oxygen data is made. It is shown that under the assumption of all ethanol converted to acetate ion, the two methods agree within 2.1% for a run of 26 hours length. The volumetric oxygen method is preferred for accuracy at low conversions and for convenience. It was therefore the method used to determine rates of reaction.

5. RESULTS AND DISCUSSION

The conversion of reactants to products in heterogeneous catalytic reactors proceeds through a well-known sequence of steps: transport of reactants from the bulk fluid to the external surface of a catalyst pellet, diffusion along the pores of the catalyst, reaction on the inner surface of the pellet, and finally diffusion and transport of the products back to the bulk stream. Any one of these steps can be the rate-limiting one, and it is of importance in reactor analyses to be able to determine the operating conditions for which a given one of the steps is controlling.

Therefore, in this chapter, the results of this study are presented and discussed in two parts. First, the results obtained from the mass transfer studies are discussed, and then the kinetic studies as well as intrapellet mass transfer studies are presented. The general method of calculations and some of the sample calculations are presented in Appendix I. The experimental and calculated data for kinetic runs are given in Appendix II.

In the following discussion, it should be particularly mentioned here that "standard reaction conditions" was defined as the liquid system consisting of 0.6 molar ethanol and 0.1 molar Na_2CO_3.

5.1 The Estimation of Diffusivity

An molecular diffusivity of oxygen under "standard reaction conditions" was estimated as follows. In the absence of data for diffusivity of oxygen in water-ethanol mixtures, the diffusivity in the liquid mixture at 25 °C was assumed equal to that in water at the same temperature[14]. The presence of dissolved Na_2CO_3 is expected to reduce the diffusivity somewhat, but the effect is probably small compared to the uncertainty in the diffusivity for the water-ethanol mixture[15]. Viscosity of the mixture was measured at 25 °C, 35 °C and 45 °C, and the diffusities at these temperatures were estimated by assuming the group $\frac{D_{AB}\mu}{T}$ is constant. The values of estimated diffusivity are presented in Table 5-1.

5.2 Mass Transfer Effects

In order to understand the kinetics of the catalytic pellet and powder system and to interpret the relation of the overall rate with respect to the concentration of dissolved oxygen, it is necessary to evaluate the rates of transfer of oxygen from gas phase to the catalyst sites. As it was already mentioned in Chapter 2, the mass transfer from the bulk gas to the gas-liquid interface was known to be rapid whereas the diffusion of the gas solute in the liquid was relatively slow. In the following sections,

the mass transfer resistance from gas-liquid interface to the bulk liquid and from the bulk liquid to the catalyst surface are discussed. The signigicance is evaluated to determine oxygen concentration at the external surface of the catalyst particles.

5.2.1 The gas-liquid mass transfer resistances

Unsteady state physical absorption experiments were carried out for the reactant gas, i.e. oxygen. By plotting the term $-\text{Ln}\left(1 - \frac{(V-V^{o})\ P_{O_2,B}}{V_L\ RT_B C_{O_2,*}}\right)$ versus time, a straight line was obtained whose slope is equal to $K_L a_g$. Details are given in Appendix I-A. The results for a solution consisting of 0.6 molar ethanol and 0.1 molar Na_2CO_3 at 25 °C and 45 °C are shown in Table I-A-1. Absorption rates were fast for these runs. Usually, no further absorption was detectable after 15 seconds. The values of $K_L a_g$ evaluated by this method were found to be:

$$K_L a_g = 1.83 \times 10^{-2} \text{ sec}^{-1} \text{ for } 25\ ^{o}C$$

$$K_L a_g = 2.58 \times 10^{-2} \text{ sec}^{-1} \text{ for } 45\ ^{o}C$$

The significance of the mass transfer resistance for absorption can then be demonstrated by the difference of the concentration at the gas-liquid interface $C_{O_2,*}$ and the

concentration of the solute gas in the bulk liquid $C_{O_2,b}$.

It is assumed that the "gas side" resistance is negligible, and the liquid at the gas-liquid interface is essentially in equilibrium with the gas. Thus, $C_{O_2,*}$ can be determined by Henry's law:

$$C_{O_2,*} = \frac{P_{O_2,r}}{H} \qquad (5\text{-}1)$$

where H is the Henry's law constant expressed in the units of atm./(g-mol/l.) and $P_{O_2,r}$ is the partial pressure of the oxygen gas in the reactor. At steady state, the rates of all mass transfer steps and the kinetic step will be the same and equal to the global rate. Hence,

$$r_v = K_L a_g \left(C_{O_2,*} - C_{O_2,b} \right) \qquad (2\text{-}3)$$

Therefore the difference in concentrations can be evaluated by equation (2-3). Details of calculations are given in the Appendix I-A. For the condition of mass transfer resistance at 25 °C, the significance of the difference in concentration represented by the percentage of $C_{O_2,*}$ is less than 0.55%.

This method was used by Kenney and Sedrik [16] in the determination of the significance of the mass transfer

resistance from the gas bubble-liquid interface to the bulk liquid in hydrogenation of crotonaldehyde over palladium catalyst. They also reported a rapid approach to saturation of the solute gas in the solvent.

It could be concluded from this study that the mass transfer resistance from the gas bubble-liquid interface to the bulk liquid is not the main and determining factor of the overall process. With a concentration difference already mentioned, this resistance can be considered small in the overall process.

5.2.2 The liquid-pellet mass transfer resistances

There is no simple experimental method which can be used to show that the mass transfer resistance from the bulk liquid to the pellet surface is negligible. However, by a fluorescent dye technique, as discussed in Sec. 4.1.2, the mass transfer coefficient could be estimated and the significance of the resistance could also be evaluated.

Average transport coefficients between the bulk stream and the pellet surface in this study could be correlated in terms of dimensionless groups which describe the flow conditions[17]. Using the mass transfer boundary layer theory and the Chilton-Colburn analogy, it could be assumed that

the mass transfer coefficient only depended on diffusivity to the 2/3 power for the same flow conditions, i.e.,

$$\frac{K_{p,Z\text{-}H_2O}}{K_{p,O_2\text{-}H_2O}} = \left(\frac{D_{Z,H_2O}}{D_{O_2,H_2O}}\right)^{2/3} \qquad (5\text{-}2)$$

where $K_{p,Z\text{-}H_2O}$ is the average mass transfer coefficient from the surface of benzoic acid to water, D_{Z,H_2O} is the molecular diffusivity of benzoic acid to water. As mentioned earlier, the diffusivity of oxygen in water-ethanol-Na_2CO_3 mixtures could be assumed equal to that in water at the same temperature. Therefore, the mass transfer coefficient K_p could be estimated for this pellet system at 25 °C.

The results and sample calculation are presented in Appendix I-B. With the mean value of K_p equal to 0.06 cm/sec, the mass transfer resistance due to this physical step represents 1.09% of the total available driving force, $C_{O_2,*}$.

As a result of the above illustration, the external resistances cause a total change of 0.55% + 1.09% = 1.64% of the equilibrium concentration, $C_{O_2,*}$. Thus, the external mass transfer resistances of this pellet system are not significant in the overall process.

5.2.3 External mass transfer resistance for powder system

In order to study the effectiveness factor of powder catalyst, the interfacial concentration, C_s, should be estimated before the Weisz parameter Φ_s and the Thiele modulus ϕ are introduced. A method is developed for estimating particle mass transfer resistance from rate measurements and is demonstrated experimentally by Ruether and Puri[6]. An external transport factor T, $T = \frac{C_s}{C_b}$, was defined[18] as a measure of external mass transfer resistance. For a system at steady state obeying power law kinetics one can equate the rate of transfer across the external film to the rate of reaction in the particle, i.e.

$$K_p A_p (C_b - C_s) = V_p K_v C_s^m \eta \qquad (5\text{-}3)$$

It is assumed here that the particle is spherical. Eq. (5-3) can then be rearranged, using previously introduced quantities and the Sherwood number, Sh, to give

$$T = \frac{Sh}{\frac{2}{3}\frac{\theta}{\tau}\eta\phi_s^2 + Sh} \qquad (5\text{-}4)$$

Eq. (5-4) can be further simplified by noting that $\eta\phi_s^2 = \Phi_s$.

One sees that as Φ_s increases with increasing speed of reaction, T decreases, indicating increased influence of external mass transfer resistance.

By doing this, one can estimate T for a first order reaction operating at $\eta = 0.8$. Brian et al [19] measured Sh for suspended particles as a function of particle diameter d and specific power input to the liquid phase. For a Schmidt number of 518, Sh ranged from 3 to 84. For this calculation one can use a conservative value of Sh = 5, which is close to the stagnant condition[17], i.e. Sh = 2. Typical values of $\theta = 0.5$ and $\tau = 3$, which are the average values of published data for Al_2O_3 shown in Table I-E-2, will also be used. For $\eta = 0.8$, $\Phi_s \doteq 3.5$. Thus for this example equation (5-4) is solved for $T = 0.93$. This indicates external mass transfer resistance is on the verge of becoming significant. For fast reaction (large Φ_s), T would decrease, and the assumption that $C_s = C_b$ would be increasingly in error. It appears, then, that $\eta \geq 0.8$ represents a reasonable estimate of the limit for which external mass transfer effects can be ignored.

On the other hand, it should be also noted that the dependence of η on D_{eff} increases with increasing speed of reaction, reaching a limit in the so called asymptotic region of the η versus ϕ function. In this region $\frac{d \ln \eta}{d \ln D_{eff}}$ $= 1/2$. In this region an error in D_{eff} of , say, 50 percent, which could easily be encountered, would give rise to an error in η of about 25 percent. An error of this magnitude would generally be considered unacceptable in the determi-

nation of kinetic data. In the limit of small values of ϕ, for which η approaches unity, η is independent of D_{eff}. For a first order reaction in a spherical catalyst at $\eta = 0.8$, $\frac{d \ln \eta}{d \ln D_{eff}} = 0.18$. In this case a 50 percent error in D_{eff} would give rise to an error in η of about 9 percent. This is suggested as a limit to acceptable uncertainty in the determination of a kinetic rate constant. Thus due to uncertainty in D_{eff} it will generally be undesirable to use data for which $\eta \leq 0.8$ to determine kinetic constants.

Using this method, the η of this study for powder systems were calculated as greater than 0.9 (Details are given in Appendix I-E). Thus, the values of T were calculated as greater than 0.974. The external mass transfer resistance, therefore, caused a total change of 2.6% of the bulk concentration, C_b.

5.2.4 The significance of intraparticle diffusion: evaluation of the effectiveness factor for crushed catalyst

Satterfield et al.[20] have considered internal diffusion resistance in heterogeneously catalyzed hydrogenation reaction

in solution. They show that it is necessary in general to consider effectiveness factors for both reactants. Because the concentration of the substrate is usually much greater than the dissolved hydrogen concentration, often both external and internal diffusion resistance for the liquid reactant is negligible. In that case the concentration of the substrate is the same in the bulk liquid, at the outer surface of the catalyst particle, and within the particle. To calculate diffusion resistance for hydrogen, the substrate concentration that appears in the kinetic rate expression may be combined with the kinetic rate constant to give a rate expression having dependence only on hydrogen concentration. This pseudo one-component kinetic rate expression is used to calculate the effectiveness factor for hydrogen in the conventional manner. Essentially, this method will also be applied in this study.

Recently, intraparticle resistance was also studied by several writers.[16,21,22,23] In all cases, the studies calculate effectiveness factors for catalyst pellets by comparing apparent rate constants for the reaction with the catalyst in the form of pellets and powder. Thus, they always assumed that the mass transfer resistance is negligible in the case of catalyst powder.

In this study calculations were performed to find the effectiveness factor of the reaction with powder catalyst

using Satterfield's method,[24] by calculating the modulus Φ_s, and the effectiveness factor was read directly from the available chart. The result shows that the effectiveness factors are greater than 0.95 at all three temperatures employed, i.e., the internal resistance can be neglected. The details of calculations are given in the Appendix I-E.

Finally, as a result of the above discussion, the oxygen concentration on the active sites of powder catalyst could be safely estimated as the concentration in bulk liquid, which could be measured by the oxygen analyzer.

5.3 Kinetic Studies

5.3.1 Calculation of reaction rates

On the catalyst powder and pellets employed in this study, oxidation occurs only within the portion where the palladium is deposited. In view of evaluating the intraparticle diffusion effects, it is necessary to relate the reaction rates to the unit catalyst volume available for the oxidation. The converted oxygen vs. time plots obtained under any given condition exhibited a linear relationship, as shown in Figure I-F-1, regardless of the form of the catalyst used. Therefore, the conversion rates are determined from the slopes of the straight lines by a linear

least squares method, and are converted to the unit volume basis of the catalyst layer. Detailed experimental data are given in Appendix II. In addition to that, by calculation, the room temperature difference of ± 0.5 °C will only cause a relative error of the oxidation rate within ± 0.17%. The chemical analysis of feed and product, mentioned earlier in section 4.2.3-(4), also confirms the reaction conversion. A sample calculation is given in Appendix I-F.

5.3.2 The reaction rates of slurry system: oxidation with the crushed pellets

Figure 5-1 shows the rates of oxidation as a function of the dissolved oxygen concentration while the concentrations of ethanol and sodium carbonate were kept at the "standard reaction conditions" in the initial solution, at each of three reactor temperatures, i.e. 25 °C, 35 °C, and 45 °C. The straight lines on this figure present the best fit of the points by the least squares method. Logarithmic plots indicated the reaction orders with respect to the dissolved oxygen concentration to be 0.92 at 25 °C, 0.97 at 35 °C, and 0.94 at 45 °C.

However, in Fig. 5-2, the oxidation rates divided by dissolved oxygen concentrations were plotted against the initial concentration of sodium carbonate at 35 °C and constant concentration of ethanol. As shown in Fig. 5-3, the divided

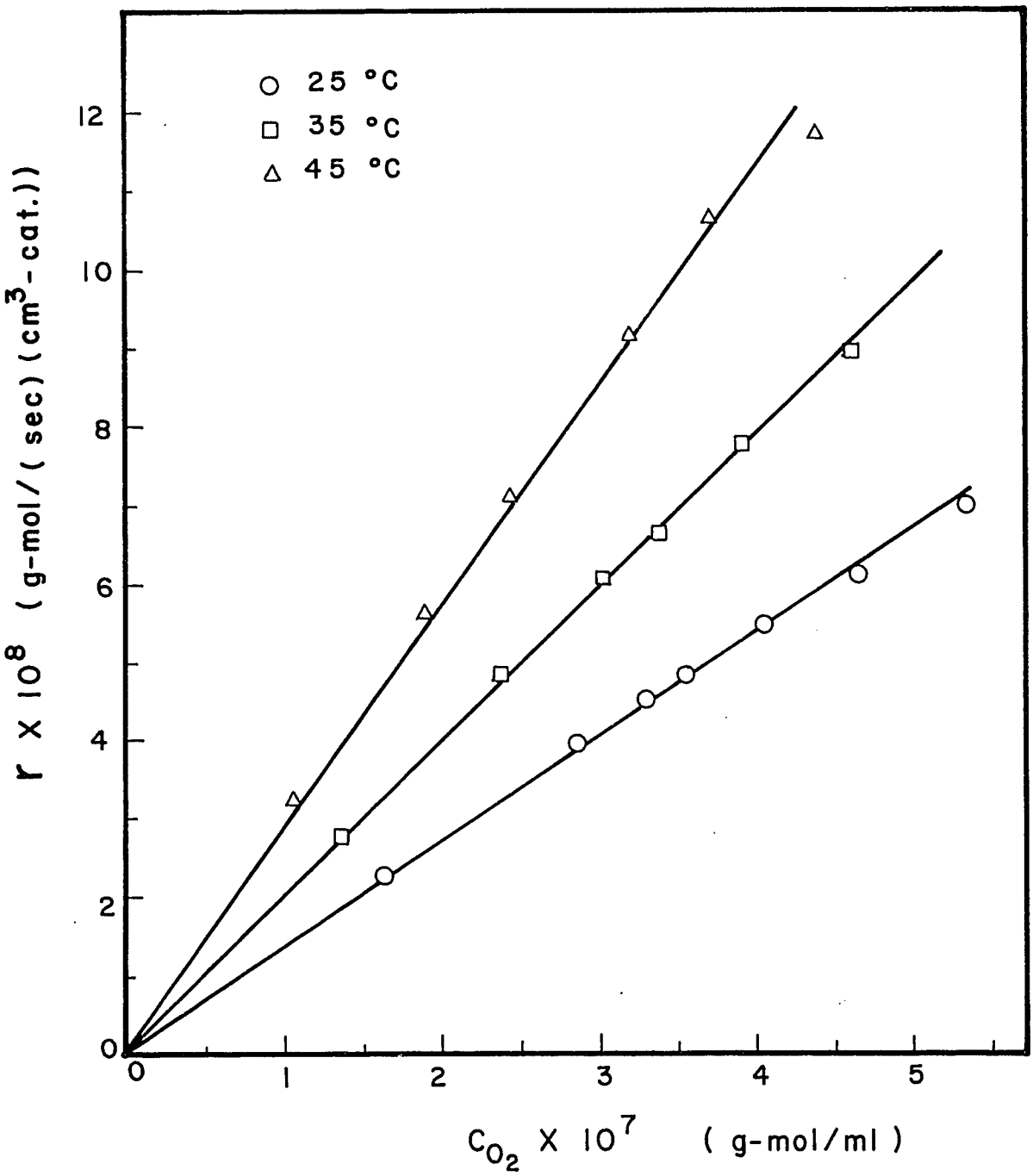

Fig. 5-1 Effect of dissolved oxygen concentration on oxidation rates with finely crushed catalyst at "standard reaction conditions".

Fig. 5-2 Dependence of modified rates on initial concentration of Na_2CO_3 at 35 ^{0}C and constant ethanol concentration (0.6 M) with crushed catalyst.

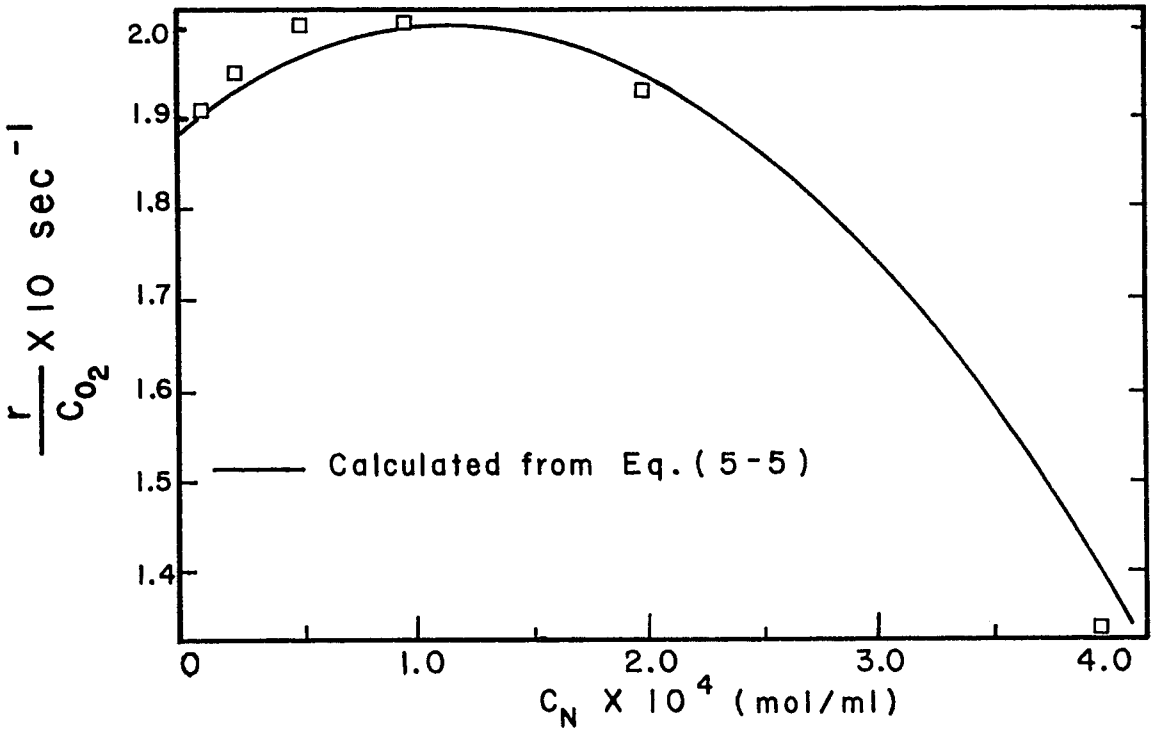

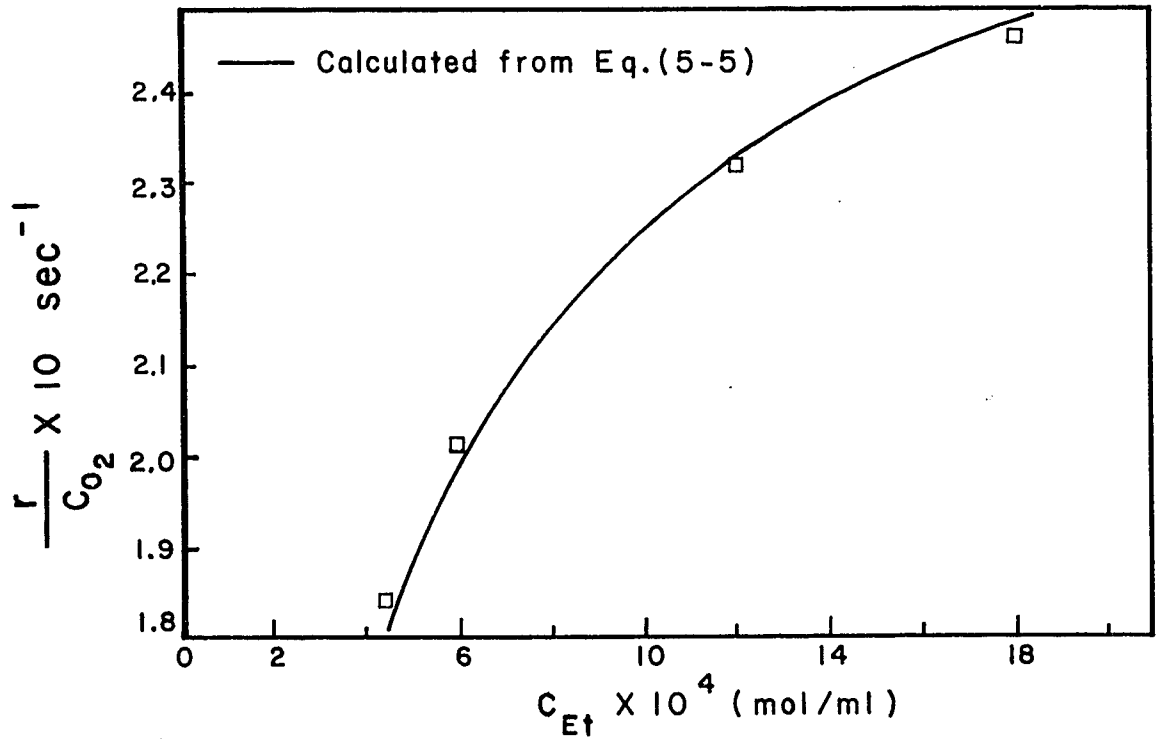

Fig. 5-3 Dependence of modified rates on initial concentration of ethanol at 35 ^{0}C and constant Na_2CO_3 concentration (0.1 M) with crushed catalyst.

ratios were also plotted against the initial concentration of ethanol at 35 °C and constant concentration of sodium carbonate. Because the oxidation rates were nearly first order in dissolved oxygen concentration, the abscissae in Fig. 5-2 and Fig. 5-3 were nearly independent of dissolved oxygen concentration. The solid lines on these two figures were calculated by Eq. (5-5) which shows the best fit of the points by a nonlinear least squares method discussed in the next section.

5.3.3 Determination of the intrinsic kinetic model

The dependence of rate on sodium carbonate concentration, as illustrated in Fig. 5-2, cannot be explained by Langumuir-Hinshelwood kinetics. A semi-theoretical analytical expression was constructed to express the rate. Terms for oxygen and ethanol concentrations are of Langumuir-Hinshelwood form, while the terms for sodium carbonate concentration are empirical. The expression is

$$r = \frac{K\, C_{O_2}\, C_{Et}}{1 + K_1\, C_{O_2} + K_2\, C_{Et}} X \left[\begin{array}{l} a_1 + a_2\, \mathrm{Ln}\,(\,1 + C_N\,) \\ - a_3\,(\,C_N + a_4\,)^{3/2} \end{array} \right] \qquad (5\text{-}5)$$

The constants were evaluated by a nonlinear least squares technique[25] from the data taken at 35 °C. The values are:

$K = 6226.278$, $K_1 = 321168.419$, $K_2 = 4409.170$, $a_1 = 0.2217$, $a_2 = 752.8$, $a_3 = 33389.6$, $a_4 = 1.0 \times 10^{-4}$.

The expression gave an average relative error compared to all data at 35 °C (14 points) of 0.98%. Even though the kinetics rate expression is relatively complex, the stable activity of $Pd\text{-}Al_2O_3$ catalyst and the fact that the stoichiometry follows a simple type of reaction without side products suggests that this may be a useful model reaction within the range of experimental variables.

Under the conditions of 35 °C and constant concentration of Na_2CO_3, C_N, Eq. (5-5) suggests that the reaction may occur directly among an adsorbed ethanol molecule and an oxygen molecule as well as a sodium carbonate molecule still in the liquid phase. Oxygen molecules may or may not be adsorbed, but in this type of reaction any adsorbed oxygen molecules do not participate in the reaction but merely reduce the amount of surface available for adsorption of active participants. Rate is proportional to the rate of impace of oxygen molecules as well as sodium carbonate molecules on adsorbed ethanol molecules. If oxygen molecules were not adsorbed, in the denominator of Eq. (5-5), the term of $K_1C_{O_2}$ would be zero.

Thus, as the result of above explanation, the oxidation

rate at 35 °C and "standard reaction conditions" consisting of 0.6 molar ethanol and 0.1 molar Na_2CO_3 was approximately first order in dissolved oxygen concentration. Similarly, the oxidation rates at "standard reaction conditions" and other reactor temperatures were treated to be first order with respect to dissolved oxygen concentration. Thus, the apparent first order rate constants, $K_{v,app\text{-}powder}$, could be calculated by the method of averages[26], and are shown in Table 5-1. Furthermore, the true kinetic rate constants of powder system, $K_{v,powder}$, could be determined by the method discussed in Appendix I-E, and are also shown in Table 5-1.

5.3.4 The reaction rates of pellet system: oxidation with the catalyst pellets

At the "standard reaction conditions", the dependence of the oxidation rates with the catalyst pellets on the dissolved oxygen concentrations are again indicated in Fig. 5-4. It follows that the reaction rates for the pellets fall to about 1/7 of those for the powder particles. Again, the logarithmic plots indicated the reaction orders with respect to the dissolved oxygen concentration to be 0.91 at 25 °C, 0.93 at 35 °C, and 0.96 at 45 °C. The apparent first order rate constants for the catalyst in the pellet form, $K_{v,app\text{-}pellet}$, were also calculated by the method of

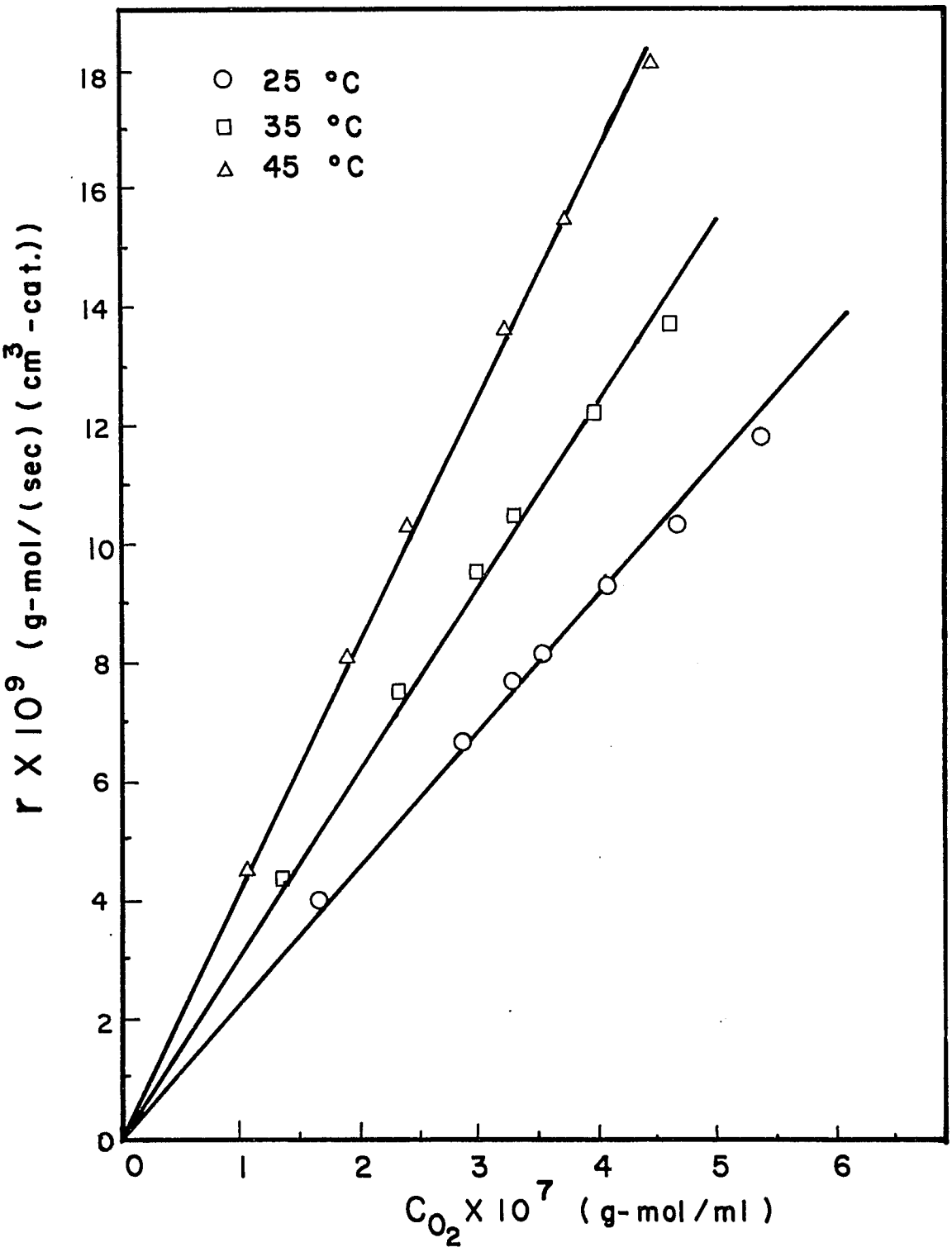

Fig. 5-4 Effect of dissolved oxygen concentration on oxidation rates with catalyst pellets at "standard reaction conditions".

averages as discussed in the previous section, and are summarized in Table 5-1. Further, figures 5-5 and 5-6 show the effects of Na_2CO_3 and ethanol concentration on the modified reaction rates, $\frac{r}{C_{O_2}}$, respectively. The solid lines on these two figures do not describe the best fit for the experimental data on each figure, but are only meant to connect the points.

The mass transfer resistance of oxygen across the liquid film surrounding the catalyst pellet was verified as being negligible, employing the correlation method discussed in Sec. 5.2.2. It can, therefore, be considered that the oxidations with the catalyst pellets are limited only by the intraparticle diffusion of oxygen. Detailed discussion is given in the next section.

5.4 The Significance of Intraparticle Diffusion For Pellet System

5.4.1 Theoretical analysis of the catalytic effectiveness factor

To simplify the quantitative analysis of the experimental data, geometry of the catalyst is approximated by an infinite slab with effective thickness L. This assumption may be reasonable because palladium is thinly deposited

Fig. 5-5 Dependence of modified rates on initial concentration of Na_2CO_3 at 35 °C and constant ethanol concentration (0.6 M) with catalyst pellets.

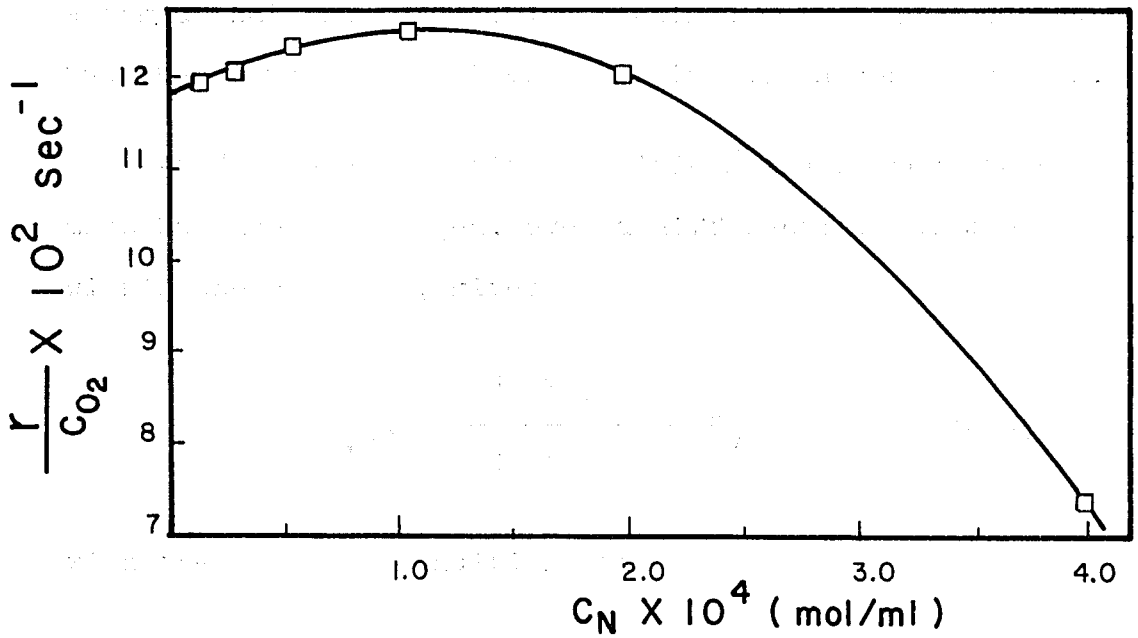

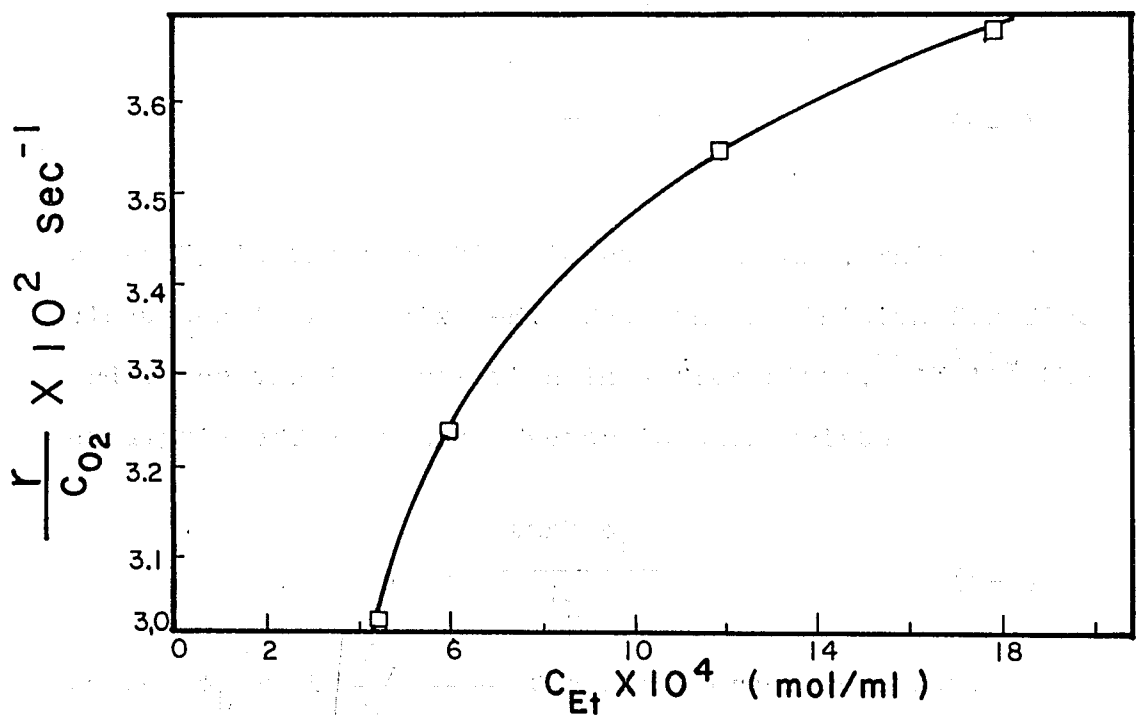

Fig. 5-6 Dependence of modified rates on initial concentration of ethanol at 35 °C and constant Na_2CO_3 concentration (0.1 M) with catalyst pellets.

on the cylindrical carrier and because the catalytic effectiveness factor is believed to be small. It is further assumed that the temperature within a pellet does not vary and that the reaction is first order in oxygen concentration.

At "standard reaction conditions" and steady state a mass balance for oxygen, over a differential thickness within the catalyst, gives

$$D_{O_2,eff} \frac{d^2 C_{O_2}}{d X^2} = K_v C_{O_2} \qquad (5\text{-}6)$$

with the boundary conditions at

$$X = 0, \quad C_{O_2} = C_{O_2,s} \qquad (5\text{-}7)$$

$$X = L, \quad \frac{d C_{O_2}}{d X} = 0 \qquad (5\text{-}8)$$

where K_v is the true kinetic rate constant, which was discussed in Appendix I-E. From the definition for first order irreversible reaction in a flat plate,[27,28,29] the catalytic effectiveness factor is then written by

$$\eta = \frac{\tanh \phi_L}{\phi_L} \qquad (5\text{-}9)$$

where $\phi_L = L\sqrt{\frac{K_v}{D_{O_2,eff}}}$ for first order reaction.

5.4.2 Determination of effectiveness factor for pellet catalyst

The following procedure can be performed to determine the effective diffusivity of oxygen, $D_{O_2,eff}$, included in ϕ_L.

First of all, the catalytic effectiveness factor is obtained taking the ratio of the apparent rate constant with the catalyst pellets to the corrected intrinsic rate constant, obtained from experiments using crushed catalyst. From this η, the corresponding modulus ϕ_L could be calculated from Eq. (5-9). The values of $D_{O_2,eff}$ are thus calculated from ϕ_L for all the experimental data. The average values of $D_{O_2,eff}$ secured at the three temperature levels are summarized in Table 5-1.

Finally, the tortuosity factors are calculated from a commonly used equation[24],

$$D_{O_2,eff} = \frac{D_{O_2}\,\theta}{\tau} \qquad (5\text{-}10)$$

and are included in Table 5-1. The computed tortuosity is essentially independent of temperature, which is expected, and is in good agreement with previously reported values for alumina supports in liquid reaction systems, as shown in Table I-E-2.

TABLE 5-1

Values for calculating τ

$\theta = 0.423$

$L = 2.821 \times 10^{-2}$ cm

Temperature (^{o}C)	25	35	45
$D_{O_2,sol.} \times 10^5$ (cm^2/sec)	2.10	2.68	3.27
$K_{v,app\text{-}pellet} \times 10^2$ (sec^{-1})	2.290	3.133	4.195
$K_{v,app\text{-}powder} \times 10$ (sec^{-1})	1.360	1.985	2.863
$K_{v,powder} \times 10$ (sec^{-1})	1.360	1.985	2.956
$\eta = \frac{K_{v,app\text{-}pellet}}{K_{v,powder}}$ (-)	0.168	0.158	0.142
ϕ_L (-)	5.945	6.330	7.049
$D_{O_2,eff} \times 10^6$ (cm^2/sec)	3.06	3.94	4.73
τ (-)	2.90	2.88	2.92

6. CONCLUSION

The liquid-phase oxidation of ethanol on a 0.5% $Pd-Al_2O_3$ catalyst was carried out in a stirred reactor with the catalyst in the form of pellets or slurry. Intrinsic kinetic studies were made of the rate measurements with the finely crushed pellets to give an expression which has the form of Eq. (5-5).

Experimental evidence and suitable calculations show that mass transfer resistances to the outside of the catalyst pellets in this stirred reactor were not significant. The effectiveness factor in the intrinsic kinetic study, using catalyst powder, was shown to be essentially unity.

The catalytic effectiveness factor for the pellet system was computed on the basis of Thiele's model which was constructed for the combined effects of the chemical reaction and the pore diffusion. By use of the relations between η vs. ϕ_L, the effective diffusivity of oxygen and the tortuosity factor of the catalyst pellet were separated from the experimental data. The tortuosities of 2.88 to 2.92 were within the range of previously published values.

7. REFERENCES

1. ϕstergaard, K., Adv. Chem. Eng., 7, 71 (1968).
2. Klassen, J., and R.S., Kirk, AIChE J., 1, 488 (1955).
3. Perry, J.H., ed., "Chemical Engineer's Handbook", 4 ed., McGraw-Hill, New York (1963).
4. Mueller, E., and K. Schwabe, Kolloid-Z., 52, 163 (1930).
5. Sato, Y., T. Hirose, F. Takahashi and M. Toda, Proceeding of the First Pacific Chemical Engineering Congress, Paper 8-3, Kyoto, Japen, 1972.
6. Ruether, J.A., and P.S. Puri, Can. J. Chem. Eng., 51, 345 (1973).
7. Reprinted with permission, from the 12 th Edition of "Standard Methods for the Examination of Water and Wastewater", American Public Health Association, Inc., 1965.
8. Satterfield, C.N., AIChE J., 21, 209 (1975).
9. Williamson, J.E., K.E. Bazaire, and C.J. Geankoplis, Ind. Eng. Chem. Fundam., 2, 126 (1963).
10. Lemay, Y., M.A. Sc. Thesis, University of Ottawa, 1974.
11. Pasto, D.J., and C.R. Johnson, "Organic Structure Determination", P. 379, Prentice-Hall, Englewood Cliffs, N.J., 1969.
12. Vogel, A.I., "A Text-book of Quantitative Inorganic Analysis", 3 ed., P. 252, Longmans, Bungay, Great Britain, 1961.

13. Lingane, J.J., "Electroanalytical Chemistry", 2nd ed., P. 93, Interscience Publishers, Inc., N.Y., 1958.

14. Sherwood, T.K., R.L. Pigford, and C.R. Wilke, "Mass Transfer", P. 26, McGraw-Hill, N.Y., 1975.

15. Gubbins, K.E., K.K. Bhatia, and R.D. Walker, Jr., AIChE J., 12, 548 (1966).

16. Kenney, C.N., and W. Sedrik, Chem. Eng. Sci., 27, 2029 (1972).

17. Smith, J.M., "Chemical Engineering Kinetics", 2nd ed., P. 362, P. 387, Mcgraw-Hill, N.Y., 1970.

18. Peterson, E.E., "Chemical Reaction Analysis", P. 50, Prentice-Hall, Englewood Cliffs, N.J., 1965.

19. Brian, P.L.T., H.B. Hales, and T.K. Sherwood, AIChE J., 15, 727 (1969).

20. Satterfield, C.N., Y.H. Ma, and T.K. Sherwood, I. Chem. E. Symp. Series No. 28 (Instn Chem. Engrs, London), 22 (1968).

21. Kawakami, K., S. Ura, and K. Kusunoki, J. Chem. Eng. Japan, 9, 392 (1976).

22. Kawakami, K., and K. Kusunoki, J. Chem. Eng. Japen, 9, 469 (1976).

23. Kawakami, K., Y. Ohgi and K. Kusunoki, J. Chem. Eng. Japen, 9, 475 (1976).

24. Satterfield, C.N., "Mass Transfer in Heterogeneous Catalysis", MIT Press, Cambridge, MA, 1970.

25. Kuester, J.L., and J.H. Mize, "Optimization Techniques with Fortran", McGraw-Hill, N.Y., 1976.

26. Jenson, V.G., and G.V. Jeffreys, "Mathematical Methods in Chemical Engineering", Academic Press Inc., London, 1963.

27. Thiele, E.W., Ind. Eng. Chem., 31, 916 (1939).

28. Wheeler, A., in Advan. Catalysis, III, 249 (1951).

29. Wheeler, A., in Catalysis, Vol. 2, P.H. Emmett, Ed., Reinhold, N.Y., 1955.

30. Reid, R.C., and T.K. Sherwood, "The Properties of Gas and Liquids", 2nd ed., P. 554, McGraw-Hill, N.Y., 1966.

31. Seidell, A., "Solubilities of Organic Compounds", Vol. II, 3 ed., P. 500, Van Nostrand, N.Y., 1941.

32. Aris, R., Chem. Eng. Sci., 6, 262 (1957).

33. Weisz, P.B., and J.S. Hicks, Chem. Eng. Sci., 17, 265 (1962).

34. Satterfield, C.N., and P.J. Cadle, Ind. Eng. Chem., Fundam., 7, 202 (1968).

APPENDICES

APPENDIX I

Methods of Calculations

I-A Calculation of Gas-Liquid Mass Transfer Coefficients

For the stirred reactor used in this study, the quantity, $K_L a_g$, which is the product of the mass transfer coefficient at the gas-liquid interface and the interfacial surface area, was determined by plotting data for gas absorption without chemical reaction according to the integrated form of the rate equation for unsteady state absorption. A derivation of such an equation is presented here.

The rate of mass transfer at the gas-liquid interface is given by the equation

$$\frac{d\,n}{d\,t} = K_L\, A\, (C_{O_2,*} - C_{O_2,b}) \qquad \text{(I-A-1)}$$

$$= K_L a_g\, V_L\, (C_{O_2,*} - C_{O_2,b}) \qquad \text{(I-A-2)}$$

Assuming ideal gas behavior one can write

$$C_{O_2,b} = \frac{n}{V_L} = \frac{(V - V^o)\, P_{O_2,B}}{R\, T_B\, V_L} \qquad \text{(I-A-3)}$$

where V^o and V are the initial volume and volume at any time as read on the bubble-meter B, respectively. For an infinitesimally small time interval, Eq. (I-A-1) can be written as

$$\frac{d\,n}{d\,t} = \frac{P_{O_2,B}}{R\,T_B}\,\frac{d\,V}{d\,t} \qquad \text{(I-A-4)}$$

Substituting from equations (I-A-3) and (I-A-4) in equation (I-A-1), and rearranging, one gets

$$\frac{d\,V}{d\,t} + K_L a_g\,V - K_L a_g\,\left(V^o + V_L \frac{R\,T_B}{P_{O,B}}\,C_{O_2,*} \right) = 0 \qquad \text{(I-A-5)}$$

This is a first order differential equation the solution of which under the boundary condition

$$V = V^o \quad \text{at } t = 0 \qquad \text{(I-A-6)}$$

is $$V = V^o + V_L \frac{R\,T_B}{P_{O_2,B}}\,C_{O_2,*} - \{ V_L \frac{R\,T_B}{P_{O_2,B}}\,C_{O_2,*}\ X$$

$$\exp\,(- K_L a_g\,t\ ) \} \qquad \text{(I-A-7)}$$

Rearranging equation (I-A-7) one gets

$$- \mathrm{Ln}\,\left(1 - \frac{V - V^o}{V_L}\,\frac{P_{O_2,B}}{R\,T_B\,C_{O_2,*}} \right) = K_L a_g\,t \qquad \text{(I-A-8)}$$

Furthermore, the value of $C_{O_2,*}$ in Eq. (I-A-8) can be obtained from the final saturated reading on oxygen analyzer.

From Eq. (I-A-8), a plot of the left hand side versus time would give a straight line which passes through the origin and has a slope equal to $K_L a_g$.

Experimental values of $K_L a_g$ were thus obtained from the gas solubility rate data at 25 °C and 45 °C. These results are presented in Table I-A-1. As an example, Fig. I-A-1 shows the data used to obtain $K_L a_g$ for the case of 25 °C. The conditions of this sample are as follows,

V_L = 2700.0 ml

T_B = Bubble-meter temperature
= Room temperature
= 24.2 °C
= 297.36 K

$P_{O_2,B}$ = Pure oxygen pressure in the bubble-meter B
= Readings of barometer and manometer
= 759.5 + 4.1 mm Hg
= 763.6 mm Hg

$C_{O_2,*} = 1.968 \times 10^{-7}$ mol/cm^3

Thus, the value of $K_L a_g$ can be determined from the slope of the figure, i.e. $K_L a_g = 1.962 \times 10^{-2}$ sec^{-1}. Agreement of the data with Eq. (I-A-8) deteriorates with increasing time. This is due to the system approaching saturation, where errors in experimental determination of dissolved gas volume are increasingly important.

TABLE I-A-1

Experimental Values of $K_L a_g$ for Liquid Containing 0.6 M Ethanol and 0.1 M Na_2CO_3 Under the System at 25 °C and 45 °C

Run No.	$K_L a_g$ X 10^2 (cm/sec)	
	25 °C	45 °C
1	1.344	1.732
2	1.747	2.190
3	2.017	2.782
4	2.272	2.351
5	1.652	3.425
6	1.962	2.985

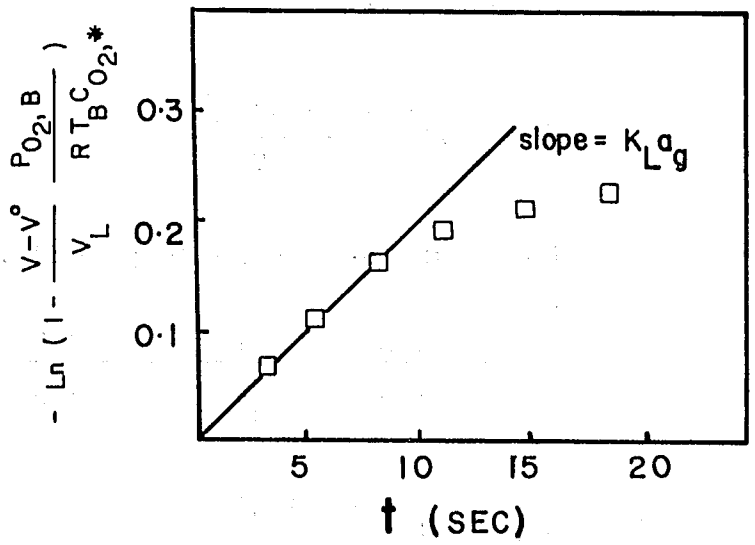

Fig. I-A-1 Plot of unsteady state absorption of oxygen in solution containing 0.6 M ethanol and 0.1 M Na_2CO_3 at 25 °C for a fixed stirring speed at 203 RPM.

I-B Calculation of Particle-Liquid Mass Transfer Coefficients

Using a fluorescent dye technique, the mass tranfer coefficient, K_p, from the pellet surface to bulk liquid can be estimated by plotting data for the rate of dissolution of benzoic acid without chemical reaction according to the integrated form of the rate equation for unsteady state dissolution. A derivation of such an equation is presented as follows.

The rate of mass transfer of benzoic acid in the liquid-pellet interface is given by the equation

$$r_p = \left(\frac{d\,n}{d\,t}\right) \frac{1}{V_L} \qquad \text{(I-B-1)}$$

$$= K_p a_p \left(C_{s,Z} - C_Z \right) \qquad \text{(I-B-2)}$$

$$= \frac{K_p\, A_p\, N_p}{V_L} \left(C_{s,Z} - C_Z \right) \qquad \text{(I-B-3)}$$

Thus, the equation can be expressed as

$$\frac{d\,C_Z}{d\,t} = \frac{1}{V_L} \frac{d\,n}{d\,t} \qquad \text{(I-B-4)}$$

$$= \frac{K_p\, A_p\, N_p}{V_L} \left(C_{s,Z} - C_Z \right) \qquad \text{(I-B-5)}$$

where K_p = the mass transfer coefficient from pellet surface to bulk liquid.

a_p = total surface area for this system per unit volume of liquid

$$= \frac{N_p \, A_p}{V_L}$$

Under the boundary condition, $C_Z = C_{Z,1} = 0$ at $t = t_1$, one can integrate on both sides and obtain

$$\int_{C_Z=0}^{C_Z} \frac{d \, C_Z}{(C_{s,Z} - C_Z)} = \int_{t_1}^{t} \frac{K_p \, A_p \, N_p}{V_L} \, d \, t \qquad \text{(I-B-6)}$$

We set $C_Z \, / \, C_{s,Z} = q$ and the equation becomes

$$\text{Ln} \left(\frac{1}{1 - q} \right) = \frac{K_p \, A_p \, N_p}{V_L} (t - t_1) \qquad \text{(I-B-7)}$$

From Eq. (I-B-7), a plot of the left hand side versus time would give a straight line; and the value of slope could be calculated. Therefore the corresponding value of K_p is given by

$$K_p = \frac{(\text{slope}) \, X \, V_L}{A_p \, N_p} \qquad \text{(I-B-8)}$$

Fig. (I-B-1) shows a sample run at 25 ^{o}C, and the values of K_p of benzoic acid to water are also shown in Table I-B-1. Consequently, using the correlation discussed is Sec. 5.2.2, the values of K_p for oxygen in the "standard reaction conditions" can be estimated and are included in Table I-B-1.

A detailed calculation can be presented as follows. Rearranging Eq. (5-2) one gets

$$K_{p,O_2\text{-sol.}} = K_{p,Z\text{-}H_2O} \left(\frac{D_{Z,H_2O}}{D_{O_2,sol.}} \right)^{-2/3} \qquad \text{(I-B-9)}$$

At 25 °C, the diffusivity of benzoic acid in water[30] 1.21 X 10^{-5} cm^2/sec and the diffusivity of oxygen in solution is 2.1 X 10^{-5} cm^2/sec. Thus, the mass transfer coefficient can be calculated by using Eq. (I-B-9), and is shown in Table I-B-1.

However, the value of a_p in this pellet system should be calculated before the mass transfer resistance from liquid to pellet surface is estimated. For the pellet catalyst used in this system, total number of pellets is 798 for 35.0075 g. Thus, one gets

$$a_p = N \times A / V_L$$

$$= 798 \times 0.5128 \text{ cm}^2 / 2700 \text{ cm}^3$$

$$= 0.15156 \text{ cm}^2/\text{cm}^3$$

Therefore, take the average value of 25 °C in Table I-B-1. One has the value of $K_{p,O_2\text{-sol.}}$ of 6.029 X 10^{-2} sec^{-1}. Thus, $K_p a_p$ of this system at the "standard reaction conditions" and 25 °C is 9.135 X 10^{-3} cm/sec.

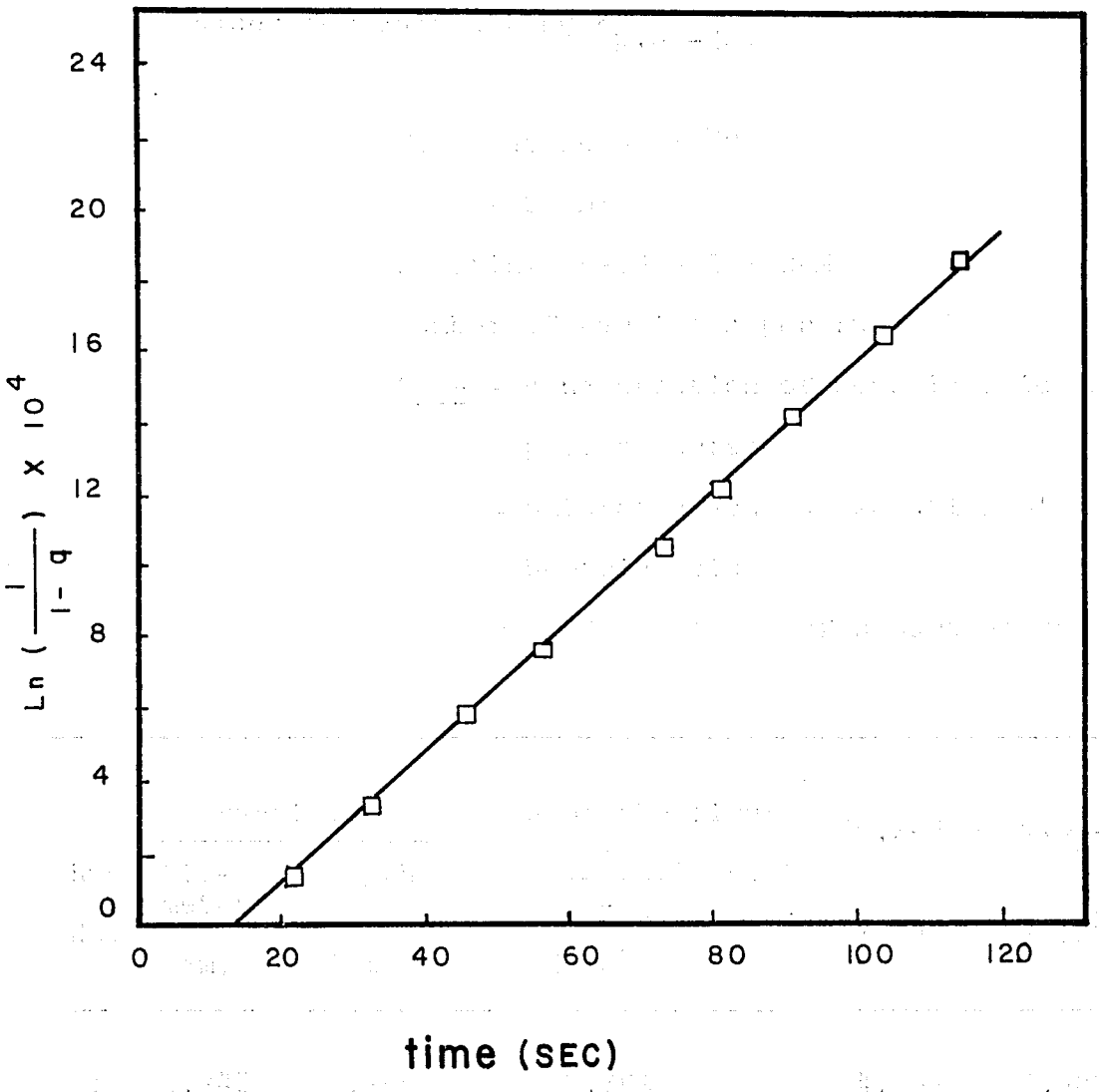

Fig. I-B-1 Plot of unsteady state dissolution of benzoic acid in water (2700 ml) at 25 °C for a fixed stirring speed at 203 RPM.

TABLE I-B-1

Values for calculating K_{p,O_2-H_2O}

Temperature = 25 °C

V_L = 2700 ml

Rotating speed = 203 RPM

Number of particles per run = 2

$C_{s,Z}$ = concentration of benzoic acid on pellet surface

= saturated aqueous solution of benzoic acid

= 0.3426 g/100 g of saturated solution[31]

Run No.	Particle Diameter (cm)	Particle length (cm)	Slope of the figure Ln $\left(\frac{1}{1-q}\right)$ vs. t X 10^5	$K_{p,Z-H_2O}$ X 10^2	K_{p,O_2-H_2O} X 10^2
1	0.348	0.355	1.753	4.093	5.907
2	0.350	0.356	1.843	4.261	6.152

I-C The Significance of the Mass Transfer Resistances for Pellet System

As mentioned earlier in Sec. 2.2, at steady state the rate equation may be written as:

$$r_v = K_L a_g \left(C_{O_2,*} - C_{O_2,b} \right) \qquad (2\text{-}3)$$

$$= K_p a_p \left(C_{O_2,b} - C_{O_2,s} \right) \qquad (2\text{-}4)$$

$$= S_m \eta \, \xi \left(C_{O_2,s} , C_{A,s} \right) \qquad (2\text{-}5)$$

The two mass transfer processes are in series. Thus,

$$\frac{1/K_p a_p}{1/K_L a_g} \left(C_{O_2,*} - C_{O_2,b} \right) = \left(C_{O_2,b} - C_{O_2,s} \right) \qquad (I\text{-}C\text{-}1)$$

Therefore the significance of the mass transfer resistance from the bulk liquid to the catalyst surface, $1/K_p a_p$, can be obtained by a comparison with the mass transfer resistance $1/K_L a_g$.

For a sample run at 25 ^{o}C, and the conditions as following:

Run No. = 2

V_L = 2700.0 cm^3

Room temperature = 23.40 ^{o}C

Barometer = 743.2 mm Hg

Manometer = 33.5 mm Hg

Catalyst weight = 35.0075 g

$C_{O_2,b} = 2.875 \times 10^{-7}$ mol/cm^3

B_{sec} = seconds needed to convert 1 cm^3 of pure oxygen gas

= 538.8 sec.

The rate of oxygen consumption can be calculated as

$$\frac{d\,n}{d\,t} = 7.794 \times 10^{-8} \text{ g-mol/sec}$$

Thus, the difference value of ($C_{O_2,*} - C_{O_2,b}$) can be estimated and the percentage of deviation from $C_{O_2,*}$ can be obtained.

Substituting the experimental data into Eq. (I-A-2), the result is:

$$\frac{d\,n}{d\,t} = K_L a_g V_L (C_{O_2,*} - C_{O_2,b}) \qquad \text{(I-A-2)}$$

$$7.794 \times 10^{-8} = (1.832 \times 10^{-2}) \times (2700.0) \times (C_{O_2,*} - 2.875 \times 10^{-7})$$

$$C_{O_2,*} = 2.891 \times 10^{-7} \text{ g-mol/cm}^3$$

and the % change of concentration due to gas-liquid resistance is:

$$\frac{C_{O_2,*} - C_{O_2,b}}{C_{O_2,*}} = \frac{1.576 \times 10^{-9}}{2.891 \times 10^{-7}} \times 100\%$$

$$= 0.545\ \%$$

While the resistance due to $1/K_L a_g$ contributes a deviation from the equlibrium concentration of 0.545%, the resistance $1/K_p a_p$ in turn, contributes a further deviation of:

$$\frac{(C_{O_2,b} - C_{O_2,s})}{C_{O_2,*}} = \frac{1/K_p a_p}{1/K_L a_g} \frac{(C_{O_2,*} - C_{O_2,b})}{C_{O_2,*}} \quad \text{(I-C-2)}$$

$$= \frac{109.473}{54.585} \text{ X } 0.545 \%$$

$$= 2.006 \text{ X } 0.545 \%$$

$$= 1.093 \%$$

The total external resistances, therefore, cause a total change of 0.545 % + 1.093 % = 1.638 % of the equilibrium concentration.

Similarly, for the pellet system at 45 °C and Run No. 24 the resistance due to $1/K_L a_g$ contributes a deviation from the equlibrium concentration of 0.692 %. It is further assumed here that the ratio of $1/K_p a_p$ to $1/K_L a_g$ at 45 °C is the same as the ratio at 25 °C, i.e. $1/K_p a_p : 1/K_L a_g = 2.006$, the resistance $1/K_p a_p$ in turn contributes a further deviation of 1.388 %. Again, the total external resistances at 45 °C cause a total change of 0.692 % + 1.388 % = 2.080 % of the equlibrium concentration. Thus, it can be concluded that the mass transfer resistances for pellet systems are not significant in the overall process.

I-D Calculation of Porosity Factor

It should be emphasized here that the effectiveness factor for catalytic reactions can depend not only on the oxtent of the void spaces, but also on the size of the openings. Therefore it is desirable to know the distribution of void volume in a catalyst according to size of the opening.

The pore-volume and surface area distribution of pellet catalyst used in this study are shown in Tables I-D-1(a) and I-D-1(b) which were supplied by the Pittsburgh Energy Research Center, U.S. Energy Research and Development Administration. Then the void fraction, or porosity, θ, of the pellet may be calculated from the equation

$$\theta = \frac{\text{void (pore) volume of pellet per gram}}{\text{total volume of pellet per gram}} \quad \text{(I-D-1)}$$

Thus, take the mean value of void volume which were shown in the Tables I-D-1(a) and I-D-1(b) to calculate the porosity of this study, i.e.

θ = pore volume of pellet X density of the pellet

= 0.272 cm^3/g X 1.556 g/cm^3

= 0.423

TABLE I-D-1 (a)

Pore-volume and Surface Area Distribution in Alumina Pellets

Range Pore Diameter, Å	Average Dia., Å	Cumulative Pore Volume (CC/G)	Cumulative Surface Area (SQ M/G)
600-500	550.0	0.004791	0.345
500-450	475.0	0.008972	0.701
450-400	425.0	0.013381	1.116
400-350	375.0	0.017930	1.601
350-300	325.0	0.023276	2.259
300-280	290.0	0.025105	2.511
280-260	270.0	0.027348	2.843
260-240	250.0	0.030301	3.316
240-220	230.0	0.033966	3.958
220-200	210.0	0.038160	4.752
200-180	190.0	0.042592	5.685
180-160	170.0	0.047769	6.903
160-150	155.0	0.050350	7.569
150-140	145.0	0.053570	8.457
140-130	135.0	0.059221	10.132
130-120	125.0	0.066089	12.330
120-110	115.0	0.074352	15.204
110-100	105.0	0.092204	22.004
100 -95	97.5	0.102423	26.199
95 -90	92.5	0.114461	31.402
90 -85	87.5	0.126873	37.076
85 -80	82.5	0.139553	43.224
80 -75	77.5	0.154191	50.780
75 -70	72.5	0.170240	59.634
70 -65	67.5	0.182269	66.762
65 -60	62.5	0.196538	75.895
60 -55	57.5	0.203416	84.158
55 -50	52.5	0.213915	92.157
50 -45	47.5	0.228950	100.505
45 -40	42.5	0.238446	109.545
40 -35	37.5	0.246891	118.552
35 -30	32.5	0.254101	127.427
30 -25	27.5	0.260644	136.944
25 -20	22.5	0.269366	152.450

TABLE I-D-1 (b)

Pore-volume and Surface Area Distribution in Alumina Pellets

Range Pore Diameter, Å	Average Dia., Å	Cumulative Pore Volume (CC/G)	Cumulative Surface Area (SQ M/G)
600-500	550.0	0.006039	0.439
500-450	475.0	0.010552	0.519
450-400	425.0	0.014478	1.189
400-350	375.0	0.018884	1.659
350-300	325.0	0.024558	2.395
300-280	290.0	0.027667	2.781
280-260	270.0	0.031031	3.280
260-240	250.0	0.034609	3.852
240-220	230.0	0.038676	4.559
220-200	210.0	0.042435	5.275
200-180	190.0	0.046302	6.089
180-160	170.0	0.051645	7.347
160-150	155.0	0.055085	8.235
150-140	145.0	0.059306	9.399
140-130	135.0	0.065732	11.303
130-120	125.0	0.074154	13.996
120-110	115.0	0.084280	17.520
110-100	105.0	0.101946	24.250
100- 95	97.5	0.112374	28.528
95 -90	92.5	0.124700	33.858
90 -85	87.5	0.136989	39.476
85 -80	82.5	0.149692	45.635
80 -75	77.5	0.164362	53.207
75 -70	72.5	0.179754	61.699
70 -65	67.5	0.191238	68.504
65 -60	62.5	0.204877	77.233
60 -55	57.5	0.216717	85.470
55 -50	52.5	0.227983	94.053
50 -45	47.5	0.237379	101.966
45 -40	42.5	0.245316	109.486
40 -35	37.5	0.253197	117.843
35 -30	32.5	0.260337	126.630
30 -25	27.5	0.266723	135.919
25 -20	22.5	0.274632	149.979

I-E Calculation of Average Effectiveness Factor

I-E.1 Introduction

A method is given for calculating an average effectiveness factor, η_{avg}, for a slurry catalyst with a distribution of particle sizes. The method is useful for determining kinetic constants from experimental data when the effectiveness factor for the largest catalyst particles cannot to be assumed equal to unity. Due to external mass transfer resistance and uncertainty in the estimation of the effective diffusivity, the method is recommended for use only when $\eta_{avg} \geq 0.8$.

I-E.2 Validation of method

Define an average effectiveness factor based on the total number of active sites, J, in the catalyst used to conduct a reaction.

$$\eta_{avg} = \frac{\sum_{j=1}^{J} N_{p,j}\, \eta_j}{\sum_{j=1}^{J} N_{p,j}} \qquad \text{(I-E-1)}$$

Let the catalyst particles be classified according to their volume per particle into N groups, with V_i the summed volume of all particles in the i'th group. If the density of active sites is independent of particle size, η_{avg} may be approximated by

$$\eta_{avg} = \frac{\sum_{i=1}^{N} V_i \eta_i}{\sum_{i=1}^{N} V_i} \qquad \text{(I-E-2)}$$

as shown by Aris.[32] If the catalyst particles may be taken as spherical, Eq. (I-E-2) becmes

$$\eta_{avg} = \frac{\sum_{i=1}^{N} N_{p,i} \bar{d}_i^3 \eta_i}{\sum_{i=1}^{N} N_{p,i} \bar{d}_i^3} \qquad \text{(I-E-3)}$$

The values of $N_{p,i}$ and $\bar{d}_i$ to be used in Eq. (I-E-3) are determined by evaluating the particle size distribution of the catalyst.

There remains the problem of evaluating the η_i in Eq. (I-E-3). From experiments, the term $\frac{-1}{V_c}\frac{dn}{dt}$ is known. If power law kinetics are followed, equivalently $K_{v,app}$, the apparent rate constant is known. An estimate of η_i could be calculated from $\phi_{s,i}$, where $\bar{d}_i$ is used for the particle size and K_v is approximated by $K_{v,app}$. If $\eta_{avg} < 1$, this method overestimates η_i for all i. A better method is to calculate η_i from $\Phi_{s,i}$,

where $\bar{d}_i$ and $K_{v,app}$ are used to evaluate $\Phi_{s,i}$. Values of η_i calculated in this way are overestimated for small $\bar{d}_i$ and underestimated for large $\bar{d}_i$. It should be noted here that the two errors tend to compensate, so that η_{avg} thus calculated is very nearly correct. The value of η_{avg} can be checked by computing a true kinetic constant according to

$$K_v = \frac{K_{v,app}}{\eta_{avg}} \qquad \text{(I-E-4)}$$

This value of K_v is used to calculate values of $\phi_{s,i}$. Eq. (I-E-3) is again employed, when η_i are now calculated from $\phi_{s,i}$. If K_v has been correctly determined, identical values of η_{avg} should be obtained when calculated in the two ways. When a correct value of η_{avg} has been computed, the experimental data are corrected according to Eq. (I-E-4) to give the true kinetic constant. As previously stated, details were discussed in Sec. 5.2.3, the method is recommended only for $\eta_{avg} \geq 0.8$.

To perform the first calculation of η_{avg} using $\Phi_{s,i}$ it is useful to have an analytical expression for η as a function of Φ_s. Although exact expressions for $\eta(\Phi_s)$ have not been reported, it is sufficient to use an empirical expression having the required accuracy over the range of Φ_s of interest.

I-E-3. Treatment of effectiveness factor for "standard reaction conditions" of powder system

As mentioned earlier in Sec. 5.3.3, the rates at "standard reaction conditions" were found to be first order in dissolved oxygen concentration. The rates were measured with whole catalyst pellets and with ground catalyst, the ground catalyst collected after passing through a sieve having 88 micron mesh opening. Catalyst internal void fraction was measured as 0.423, specific area as 151 m^2/g, and pellet density as 1.557 g/cm^3. The apparent first order rate constants for catalyst in the form of pellets and powder are shown in Table I-E-1. It was thus apparent that the measured effectiveness factor for the pellets was substantially less than unity. It was necessary to determine next whether the apparent first order rate constant measured for the powder gave the true kinetic constant.

The way to estimate diffusivity of this study was discussed previously in Sec. 5.1, and shown in Table I-E-1. Table I-E-2 shows some experimental determinations of the tortuosity factor for alumina used in each case to support a platinum series metal catalyst similar to the one used in this work. The variation in reported values of τ is considerable. Initially, an average of the values in Table I-E-2 was used, $\tau = 2.8$. Thus, the effective diffusivities were estimated as shown in Table I-E-1. The Weisz para-

meters Φ_s were calculated[33] using the largest diameter, i.e. d_{max} = 88 microns. Then the results were shown in Table I-E-1. Thereupon, the effectiveness factor was read directly from the avilable chart.[24] For the cases at 25 °C and 35 °C it was not necessary to determine the particle size distribution. To the accuracy to which D_{eff} can be estimated, the effectiveness factors for the powdered catalyst at 25 °C and 35 °C are unity. However, this method based on the largest particle is not adequate for the powder system at 45 °C because the value of $\Phi_{s,\ 45\ ^oC}$ is greater than 1., i.e. the intraparticle resistance cannot be neglected. The more rigorous approach employing the catalyst particle distribution is necessary for the powder system at 45 °C.

Experimental data for the particle size distribution of the powdered catalyst are shown in Table I-E-3. By inspection of the final column in Table I-E-3 one sees that only 2/14 of the total sites in the catalyst are found in particles as large as the sieve opening, 88 microns.

As mentioned above, to employ equation (I-E-3) with $\Phi_{s,i}$ to calculate η_i it is convenient to have an analyticl expression for η as a function of Φ_s. The following expression for a first order reaction gives η to one percent accuracy for $\eta \geq 0.4$.

$$\log_{10} \eta = 0 \quad \text{for } \log_{10} \Phi_s < -0.800 \quad \text{(I-E-5)}$$

$$\log_{10} \eta = -0.0923 \left(\log_{10} \Phi_s \right)^3 - 0.0971 \left(\log_{10} \Phi_s \right)^2 - 0.0545 \log_{10} \Phi_s - 0.0287$$

$$\text{for } \log_{10} \Phi_s \geq -0.800 \quad \text{(I-E-6)}$$

When Eq. (I-E-3) is used to calculate η_{avg} by means of $\Phi_{s,i}$ the result is $\eta_{avg} = 0.9690$. The true kinetic constant is estimated using $K_v = K_{v,app} / 0.9690 = 0.2954 \text{ sec}^{-1}$ (I-E-7)

The value of K_v given in Eq. (I-E-7) is used to calculate values of $\phi_{s,i}$, and η_{avg} is again calculated using Eq. (I-E-3) and following equation

$$\eta_i = \frac{3}{\phi_{s,i}} \left\{ \frac{1}{\tanh \left(\phi_{s,i} \right)} - \frac{1}{\phi_{s,i}} \right\} \quad \text{(I-E-8)}$$

One finds again that $\eta_{avg} = 0.9704$. Thus the initial estimate of η_{avg} could be accepted within one percent accuracy, and the kinetic rate constant is given by Eq. (I-E-7), i.e., $K_v = 0.2954 \text{ sec}^{-1}$ for the powder system at 45 ^{o}C. But this K_v is calculated based on published data of tortuosity for Al_2O_3.

In order to get the tortuosity factor of this study, one can use $K_v = 0.2954\ sec^{-1}$ from the above method and apply the method in Sec. 5.4.2 to estimate a corrected value of tortuosity factor, i.e. $\tau = 2.92$. Again, using the method presented in this section with $\tau = 2.92$, one has $\eta_{avg} = 0.9683$. Also, using Equations (I-E-3) and (I-E-8), one has $\eta_{avg} = 0.9694$. Thus, the true kinetic constant is estimated using Eq. (I-E-4), i.e.

$$K_v = \frac{K_{v,app}}{\eta_{avg}} = \frac{0.2863}{0.9683} = 0.2956\ sec^{-1}$$

Finally, this $K_v = 0.2956\ sec^{-1}$ can be used in Sec. 5.4.2. Again one gets the same $\tau = 2.92$. Therefore, $K_v = 0.2956\ sec^{-1}$ can be treated as the true kinetic constant for the powder system at 45 ^{o}C of this study.

TABLE I-E-1

Values of Weisz Modulus Φ_s at $\tau = 2.8$ and $d_{max} = 88$ micron

$\theta = 0.423$

$d_{max} = 88$ micron

$\tau = 2.8$

Temperature (^{o}C)	25	35	45
$K_{v,app\text{-}powder} \times 10$ (sec^{-1})	1.360	1.985	2.863
$D_{O_2,sol.} \times 10^5$ (cm^2/sec)	2.10	2.68	3.27
$D_{O_2,eff} \times 10^6$ (cm^2/sec)	3.17	4.06	4.94
$\Phi_s = \frac{d_{max}^2}{4 D_{O_2,eff}} \left(\frac{-1}{V_c} \frac{dn}{dt} \right) \frac{1}{C_s}$			
$= \frac{d_{max}^2}{4 D_{O_2,eff}} (K_{v,app\text{-}powder})$	0.83	0.95	1.12

TABLE I-E-2

Specific Surface Area, Tortuosity Factor, and Internal Void Fraction for Alumina Pellets

Area, M^2/g	τ	θ	Authors
197	3.9	0.585	23
100	2.8	0.56	20
265	1.6	0.54	15
6.4	2.8	0.389	34

TABLE I-E-3 Catalyst Particle Size Distribution:
Approximately 2.5 mg Crushed Catalyst

i	Particle Diameter Range, Micron	$\bar{d}_i$, micron	$N_{p,i}$	$N_{p,i}\bar{d}_i^3 \times 10^{-3}$ (micron)^3
1	0-12	6	328	70.8
2	12-20	16	156	639
3	20-28	24	127	1,756
4	28-36	32	74	2,425
5	36-44	40	21	1,344
6	44-60	52	24	3,375
7	60-88	74	5	2,026
8	88-92	90	3	2,187
9	>92	---	0	0
				13,823

I-F Calculation of the Reaction Rates

I-F.1 Sample calculation for oxygen consumption

The sample calculation below is for one of the runs at "standard reaction conditions" and 45 °C. The calculation is based on the assumption of the ideal gas law, and assumes that the temperature of oxygen in the bubble-meter is the same as room temperature. Furthermore, the dissolved oxygen concentration for each run was kept at constant reading while the reaction proceeded. Thus, the partial pressure of oxygen in the reactor could be assumed constant for each run.

The reaction rates were obtained by measuring the rate of oxygen consumption. From the stoichiometry of the reactions studied, one mole of oxygen is required for one mole of substrate. The reaction rate is thus given by the expression of oxygen consumption. Therefore,

$$\frac{d\,n}{d\,t} = \left(\frac{P_{O_2,B}}{R\,T_B}\right) \frac{d\,V}{d\,t} \qquad \text{(I-F-1)}$$

where $P_{O_2,B}$ is the summation of readings on barometer and manometer.

For Run No. 26, reactor temperature is 45 °C, and

$$P_{O_2,B} = 785.4 \text{ mm Hg}$$

$$T_B = 23.53 \text{ °C}$$

As shown in Fig. I-F-1, a slope could be calculated by a

linear least squares method, i.e.,

$$\frac{d\,V}{d\,t} = \frac{1}{B_{sec}} = \frac{1}{203.1}\ \frac{cm^3}{sec}$$

Thus,
$$\frac{d\,n}{d\,t} = \frac{P_{O_2,B}}{R\,T_B}\ \frac{1}{B_{sec}}$$

$$= \frac{785.4/760.0}{82.0567 \times 296.68} \times \frac{1}{203.1}$$

$$= 2.090 \times 10^{-7}\ \text{mol/sec}$$

For the pellet system, the total weight of catalyst pellets is 35.0075 g, and the bulk pellet density is 1.556 g/cm^3. Also, the volume of palladium catalyst layer corresponded to 51.3% of the total pellet volume. Therefore, the reaction rate could be converted to the unit volume basis of the catalyst layer. Thus,

$$r = \left(\frac{d\,n}{d\,t}\right)\frac{\rho_p}{W} \times \frac{1}{51.3\ \%}$$

$$= 2.090 \times 10^{-7} \times \frac{1.556}{35.0075} \times \frac{1}{51.3\ \%}$$

$$= 1.810 \times 10^{-8}\ \text{mol/(sec)(cm}^3\text{-cat)}$$

In order to confirm that the reaction rate can be measured by the consumption of oxygen, the conversion of sodium carbonate was also tested by chemical analysis and is shown in the next section.

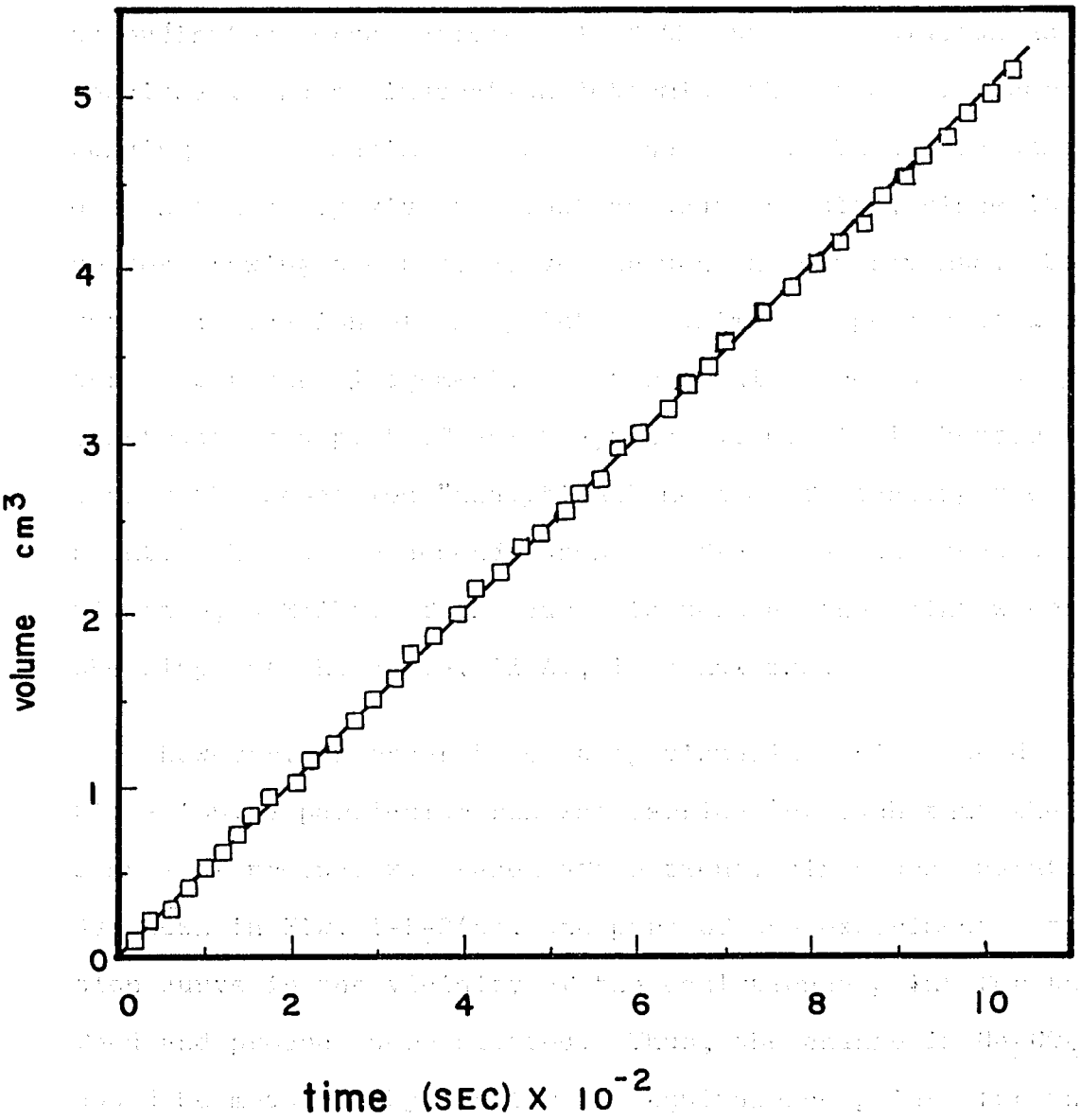

Fig. I-F-1 Oxygen consumption versus time for Run No. 26 at 45 °C.

I-F.2 Potentiometric titrations

As mentioned earlier in Sec. 4.2.3-(4), an obvious method of finding the equivalence point is to plot e.m.f. (E) values as ordinates versus volume (V) of the titrant solution as abscissae, and by inspection determine the value of V corresponding to the maximum slope of the curve. This procedure does not usually give the most accurate results, since it involves drawing the best curve through the experimental observations; location of the point of maximum slope may be a matter of personal judgement. Better results are obtained by constructing a plot of $\Delta E/\Delta V$ against V, but it is better to employ the so-called "analytical" method of locating the end point.[13] The latter depends upon the fact that the second derivative, $\Delta^2 E/\Delta V^2$, of the curve is zero at the point where the slope of the curve, $\Delta E/\Delta V$, is a maximum.

However, in order to clearly visualize this method of titration, a particular run was carried out such that the sample of product was taken after twenty six hours operation. As shown in Fig. I-F-2(a), the part of the experimental titration curve in the vicinity of the equivalence point for the feed and product were plotted. Thus, the change in Na_2CO_3 could be measured by finding the equivalence points for these two titration curves by the means of "analytical" method. As shown in Fig. I-F-2(b), the second derivation becomes zero at the inflexion point and provides a more exact measurement of the equivalence point for the feed and product respectively.

The sample calculation were given as follows. At Run No. 26, as shown in previous section, the reaction rate was calculated as 7.524×10^{-4} mol/hr. Thus, it could be estimated that the total consumption of carbonate ions will be $7.524 \times 10^{-4} \times 26 = 1.956 \times 10^{-2}$ mol in the reactor after twenty six hours operation.

Using the glass-electrode and saturated calomel electrode pH meter, 50.0 ml of feed solution were titrated with standard 0.0508 N acetic acid; and the end-point volume was found at 98.56 ml (as shown in Fig. I-F-2). Similarly, 50.0 ml of product were also found the end-point volume at 91.58 ml. Therefore, the total consumption of carbonate ions in 2.7 liters solution could be calculated, i.e.,

$$\frac{(98.56 - 91.58) \times 0.0508}{50.0} \times 2.7 = 1.915 \times 10^{-2} \text{ mol}$$

and compare to the value of oxygen consumption, the relative error is 2.1 %.

As a result of above discussion, it should be concluded here that the reaction rate in this study could be measured either by oxygen consumption or by sodium carbonate consumption.

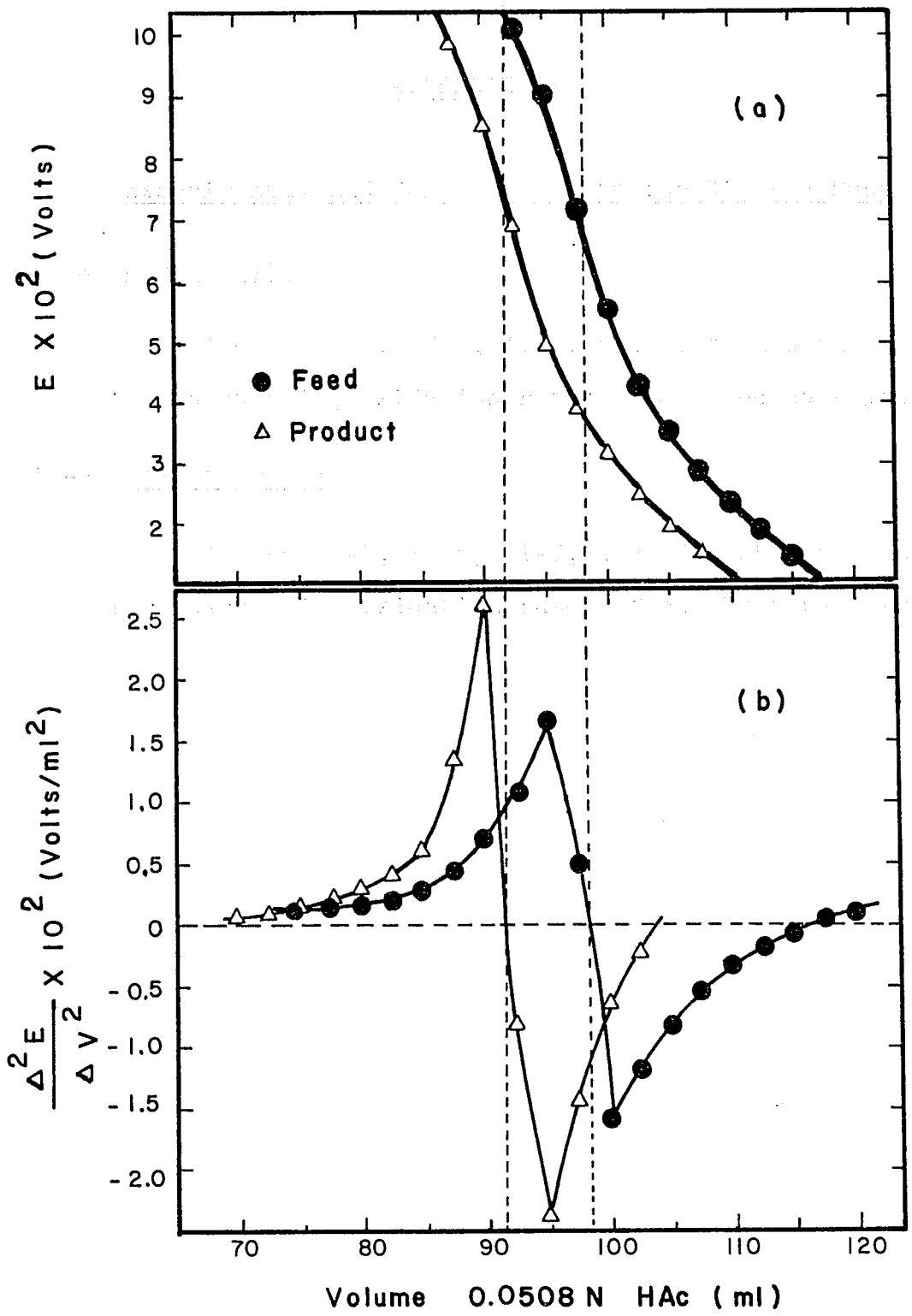

Fig. I-F-2 (a) e.m.f. (E) versus volume (V) for potentiometric titration.

(b) $\Delta^2E/\Delta V^2$ versus V.

APPENDIX II

Experimental and Calculated Data for Kinetic Runs

II-A Slurry system

Tables II-1, II-2, II-3, and II-4 show the data for calculating oxidation rates of crushed catalyst.

II-B Pellet system

Tables II-5, II-6, II-7, and II-8 show the data for calculating oxidation rates of catalyst pellets.

TABLE II-1

Slurry System: Reaction Rate With Respect to Substrate Concentrations At the "Standard Reaction Conditions" and 25 ^{o}C

Run No.	W	$P_{O_2,B}$	T_B	B_{sec}	$C_{O_2} \times 10^7$	$r \times 10^8$
	g	mm Hg	^{o}C	sec	mol/cm^3	$mol/(sec)(cm^3\text{-cat})$
51	10.023	791.7	23.35	541.3	1.659	2.392
52	10.316	780.1	23.37	309.8	2.900	4.002
53	10.285	796.5	23.32	279.2	3.344	4.548
54	10.983	789.2	23.35	241.7	3.569	4.874
55	10.212	784.2	23.38	227.6	4.109	5.531
56	10.830	787.0	23.35	192.3	4.700	6.196
57	8.103	792.3	23.35	227.8	5.375	7.037

TABLE II-2

Slurry System: Reaction Rate With Respect to Substrate Concentrations At the "Standard Reaction Conditions" and 35 ^{o}C

Run No.	W	$P_{O_2,B}$	T_B	B_{sec}	C_{O_2} X 10^7	r X 10^8
	g	mm Hg	^{o}C	sec	mol/cm^3	mol/(sec)(cm^3-cat)
61	8.792	795.0	23.50	527.7	1.406	2.828
62	7.457	784.9	23.40	355.2	2.406	4.857
63	5.272	791.2	23.38	402.7	3.069	6.110
64	5.983	784.4	23.56	320.6	3.422	6.700
65	5.053	792.2	23.36	328.5	3.938	7.824
66	4.873	791.0	23.35	295.4	4.641	9.020

TABLE II-3

Slurry System: Reaction Rate With Respect to Substrate Concentrations At the "Standard Reaction Conditions" and 45 ^{o}C

Run No.	W	$P_{O_2,B}$	T_B	B_{sec}	$C_{O_2} \times 10^7$	$r \times 10^8$
	g	mm Hg	^{o}C	sec	mol/cm^3	$mol/(sec)(cm^3\text{-cat})$
71	8.177	798.6	23.42	485.3	1.119	3.299
72	7.055	781.7	23.35	321.7	1.919	5.647
73	7.232	787.3	23.38	248.6	2.472	7.177
74	7.383	796.8	23.35	190.9	3.231	9.269
75	7.208	783.9	23.41	166.0	3.737	10.740
76	7.216	788.1	23.38	151.9	4.469	11.787

TABLE II-4

Slurry System: Reaction Rate With Respect to Substrate Concentrations at 35 ^{o}C

Run No.	W g	$P_{O_2,B}$ mm Hg	T_B ^{o}C	B_{sec} sec	$C_N \times 10^4$ mol/cm^3	$C_{Et} \times 10^4$ mol/cm^3	$C_{O_2} \times 10^7$ mol/cm^3	$r \times 10^8$ mol/(sec)(cm^3-cat)
80	5.227	796.7	23.34	474.9	1.0	18.0	2.140	5.263
81	5.274	790.6	23.34	476.1	1.0	12.0	2.221	5.163
62	7.458	784.9	23.40	355.2	1.0	6.0	2.406	4.857
83	5.012	787.2	23.36	559.2	1.0	4.5	2.500	4.604
90	5.376	795.4	23.36	809.7	4.0	6.0	2.250	3.012
91	4.243	795.9	23.35	675.4	2.0	6.0	2.360	4.554
93	4.385	791.1	23.37	608.7	0.5	6.0	2.425	4.858
94	4.264	791.7	23.35	631.7	0.2	6.0	2.481	4.819
95	4.185	784.8	23.36	643.2	0.1	6.0	2.509	4.780

TABLE II-5

Pellet System: Reaction Rate With Respect to Substrate Concentrations At the "Standard Reaction Conditions" and 25 ^{o}C

W = 35.0075 g

Run No.	$P_{O_2,B}$ mm Hg	T_B ^{o}C	B_{sec} sec	$C_{O_2} \times 10^7$ mol/cm^3	$r \times 10^9$ mol/(sec)(cm^3-cat)
1	782.8	23.65	906.2	1.672	4.041
2	776.7	23.40	538.8	2.875	6.750
3	797.1	23.35	484.6	3.313	7.702
4	798.2	23.60	495.6	3.563	8.127
5	800.1	23.58	401.7	4.131	9.320
6	795.7	23.35	359.0	4.719	10.380
7	790.2	23.58	311.1	5.400	11.886

TABLE II-6

Pellet System: Reaction Rate With Respect to Substrate Concentrations At the "Standard Reaction Conditions" and 35 ^{o}C

W = 35.0075 g

Run No.	$P_{O_2,B}$ mm Hg	T_B ^{o}C	B_{sec} sec	C_{O_2} X 10^7 mol/cm^3	r X 10^9 mol/(sec)(cm^3-cat)
11	775.6	23.65	824.1	1.359	4.403
12	775.8	23.45	483.2	2.300	7.517
13	779.0	23.34	380.8	2.994	9.581
14	799.4	23.38	356.1	3.397	10.512
15	796.2	23.35	305.2	4.003	12.218
16	799.3	23.37	272.9	4.656	13.716

TABLE II-7

Pellet System: Reaction Rate With Respect to Substrate Concentrations At the "Standard Reaction Conditions" and 45 ^{o}C

W = 35.0075 g

Run No.	$P_{O_2,B}$ mm Hg	T_B ^{o}C	B_{sec} sec	C_{O_2} X 10^7 mol/cm^3	r X 10^9 mol/(sec)(cm^3-cat)
21	794.7	23.35	810.7	1.063	4.591
22	780.5	23.35	450.2	1.919	8.119
23	784.7	23.35	356.4	2.444	10.314
24	791.5	23.37	271.5	3.250	13.625
25	797.6	23.36	240.7	3.719	15.518
26	785.4	23.52	203.1	4.500	18.100

TABLE II-8

Pellet System: Reaction Rate With Respect to Substrate Concentrations at 35 ^{o}C

W = 35.0075 g

Run No.	$P_{O_2,B}$ mm Hg	T_B ^{o}C	B_{sec} sec	$C_N \times 10^4$ mol/cm^3	$C_{Et} \times 10^4$ mol/cm^3	$C_{O_2} \times 10^7$ mol/cm^3	$r \times 10^9$ mol/(sec)(cm^3-cat)
30	742.5	23.70	479.8	1.0	18.0	2.094	7.726
31	782.7	23.72	482.5	1.0	12.0	2.131	7.588
12	775.8	23.45	483.2	1.0	6.0	2.300	7.517
33	795.2	23.65	505.1	1.0	4.5	2.431	7.366
40	798.8	23.68	603.1	4.0	6.0	2.275	6.188
41	795.0	23.55	494.5	2.0	6.0	2.344	7.524
43	779.7	23.48	469.6	0.5	6.0	2.406	7.772
44	788.4	23.48	470.2	0.2	6.0	2.447	7.849
45	788.0	23.68	455.5	0.1	6.0	2.531	8.093